ISPRS Journal of Photogrammetry and Remote Sensing 166 (2020) 95–117

Contents lists available at ScienceDirect

ISPRS Journal of Photogrammetry and Remote Sensing

journal homepage: www.elsevier.com/locate/isprsjprs

Development and application of a new mangrove vegetation index (MVI) for rapid and accurate mangrove mapping

Alvin B. Baloloy[a,*], Ariel C. Blanco[a,b], Raymund Rhommel C. Sta. Ana[a], Kazuo Nadaoka[c]

[a] Training Center for Applied Geodesy and Photogrammetry, University of the Philippines-Diliman, Quezon City 1101, Philippines
[b] Department of Geodetic Engineering, University of the Philippines, Diliman, Quezon City 1101, Philippines
[c] Department of Transdisciplinary Science and Engineering, Tokyo Institute of Technology, Tokyo, Japan

ARTICLE INFO

Keywords:
Mangrove index
Mangrove extent
Sentinel-2
Landsat
Vegetation mapping
Philippines

ABSTRACT

Advancement in Remote Sensing allows rapid mangrove mapping without the need for data-intensive methodologies, complex classifiers, and skill-dependent classification techniques. This study proposes a new index, the Mangrove Vegetation Index (MVI), to rapidly and accurately map mangroves extent from remotely-sensed imageries. The MVI utilizes three Sentinel-2 bands green, Near Infrared (NIR) and Shortwave Infrared (SWIR) in the form |NIR-Green|/|SWIR-Green| to discriminate the distinct greenness and moisture of mangroves from terrestrial vegetation and other land cover. Spectral band analysis shows that the |NIR-Green| part of MVI captures the differences of greenness between mangrove forests and terrestrial vegetation. The |SWIR-Green| part of the index expresses the distinct moisture of mangroves without the need for additional intertidal data and water indices. The MVI value increases with the increasing probability of a pixel being classified as mangroves. Eleven mangrove forests in the Philippines and one mangrove park in Japan were then mapped using MVI. Accuracy assessment was done using field inventory data and high-resolution drone orthophotos. MVI have successfully separated the mangroves from other cover especially terrestrial vegetation, with an overall index accuracy of 92%. The MVI was applied to Landsat 8 images using the equivalent bands to test the universality of the index. Comparable MVI mangrove maps were produced between Sentinel-2 and Landsat images, with an optimal minimum threshold of 4.5 and 4.6, respectively. MVI can effectively highlight the greenness and moisture information in mangroves as reflected by its moderate to high correlation value ($r = 0.63$ and 0.84, $\alpha = 0.05$) with the Sentinel-derived chlorophyll-a (C_a) and canopy water (C_w) biophysical products. This study developed and implemented two automated platforms: an offline IDL-based 'MVI Mapper' and an online Google Earth Engine-based MVI mapping interface. The MVI implemented in Google Earth Engine was used in generating the latest mangrove extent map of the Philippines. Additionally, the application of MVI were tested to four additional mangrove forests in Southeast Asia: Thailand, Vietnam, Indonesia and Cambodia; and to selected mangroves forests in South America, Africa and Australia.

1. Introduction

Mangrove forests provides several ecosystem services and coastal area protection for the tropical and subtropical coastlines of the world (Veettil et al., 2018). It supports high floral and faunal biodiversity and provide a diverse range of goods to coastal communities. Despite their importance, mangrove forests continue to decline primarily due to anthropogenic causes. Over the past 50 years, approximately one-third of the world's mangrove forests have been lost (Clough, 1993; Diop, 1993; Spalding et al., 1997; Alongi, 2002) due to factors such as conversion to aquaculture (Primavera, 2000; Primavera, 2005; Farnsworth and Ellison, 1998), sea level rise (Crooks et al., 2011; Field, 1995), urban development (Romañach et al., 2018), overexploitation for timber (Kathiresan and Bingham, 2001) and natural disturbance including typhoons (Villamayor et al., 2016; Cahoon et al., 2003) and increase in precipitation patterns and intensity (Field, 1995; Ellison, 2000). Mangrove extent monitoring is therefore significant to detect the historical and current distribution of mangroves as affected by these threats. Accurate spatial information of mangrove forest extent is essential for both land-use planning and natural resources management.

Remote sensing has been a popular tool used in mangrove forest mapping, allowing estimation and publication of global estimates (FAO, 2003; Spalding et al., 1997). It offers an inexpensive alternative to field-based techniques which are only practical at the local scale. Remote Sensing allowed scientists and planners to observe real changes in the areal extent and spatial pattern of mangrove forests over the years. In

* Corresponding author.

https://doi.org/10.1016/j.isprsjprs.2020.06.001
Received 29 January 2020; Received in revised form 12 April 2020; Accepted 1 June 2020
Available online 11 June 2020

the Philippines, Long and Giri (2011) have mapped the spatial distribution and areal extent of the mangroves in year 2000 using Landsat data and Iterative Self-Organizing Data Analysis Techniques (ISODATA) clustering. They reported a nationwide baseline extent of 268,996 ha in 1990, 256,185 ha in 2000, and 240,824 ha in 2010, showing a downward trend with almost 11% decline. The Bureau of Forest Development, now known as Forest Management Bureau, provided an extent estimate from year 1969 to 1984. Larger mangroves areas were reported in earlier years between 1918 (450,000 ha) to 1968 (448,310) (PCAFNRRD, 1991 and Lawas, 1974) which have significantly reduced to 220,984 ha in 2016 as reported by Global Mangrove Watch. The decline was attributed to overexploitation in coastal villages as brought by industrial activities and conversion to agriculture (Primavera, 2000). There are discrepancies in the estimates from different references as different satellite data and processing methods were used. Most of these misclassifications were observed in the Landsat-based estimates, including mangroves classified as water within small mangroves stands (Ghandi and Jones, 2019; Long and Giri, 2011).

New mapping techniques are still being developed due to the limitations observed from previous proposed methodologies. In supervised and non-supervised mangrove classification techniques, there is the challenge in collecting and selecting training data from remotely-sense images. Aside from selecting the most appropriate imagery, the classification method must be highly considered (Lu and Weng, 2007). The classification accuracy of different classifiers varies among different studies on mangrove vegetation mapping such as Maximum likelihood classification (MLC) versus Support Vector Machine (SVM) (Deilmai et al., 2014; Kanniah et al., 2015), Artificial Neural Network (ANN) and Random Forest (RF) versus MLC and SVM (Ma et al., 2017; Sikdar et al., 2016) and ISODATA versus MLC (Giri and Muhlhausen, 2008; Roslani et al., 2003). It is difficult to derive generalized research results due to differences in input data and study sites. Selection of region-of-interests (ROIs) are prone to biases and is affected by the user's skill in identifying mangroves versus non-mangrove pixels. Users are also limited by the capacity of the computers needed in performing the mapping operations, including the availability of enough memory and storage to handle big data and collection of satellite images. Research studies on simplifying mangrove mapping methodologies and implementing the workflow on automated and cloud-based mapping is still lacking.

Spectral indices used in mapping vegetation are called vegetation indices. These indices such as the normalized difference vegetation index (NDVI, Rouse et al., 1973), Soil Adjusted Vegetation Index (SAVI, Huete, 1988), and Leaf Area Index (LAI) can highlight plant intrinsic properties that are well related to leaf greenness and vigor. Each index has its specific expression which can represent vegetation properties better than using individual bands. However, these known indices are not specific for mangroves and cannot alone discriminate mangroves from terrestrial vegetation (Winarso et al., 2014). Mangroves and dense terrestrial mangroves may generate the same NDVI values and thus, separating them from remotely-sense images is difficult unless additional input data will be introduced. Some studies utilized elevation data (Liu et al, 2008) and tasselled cap transformation (Razali et al., 2019; Zhang and Tian, 2013) to further improve the classification accuracy. To address the challenge in mapping mangroves with the vegetation indices, some researchers have proposed mangrove-specific vegetation indices using different inputs bands and satellite data. One of which is the Mangrove Index (MI) proposed by Winarso et al. (2014). It was first applied in Alas Purwo Mangrove area, Banyuwangi East Java Province, Indonesia utilizing both Landsat-8 Near Infrared (NIR) and Shortwave Infrared (SWIR) bands (see Table 1). The formula were tested on other data such as Landsat ETM + by incorporating different multiplication factor as modified to the radiometric resolution of the data. The authors have used MI together with NDVI image to detect degraded and non-degraded mangroves sites. Similar NDVI and MI pattern indicates areas in good condition, while opposite pattern indicates a degraded one. In term of MI values, high values indicate healthy mangroves. The study acquired field survey data but the accuracy of delineating the mangroves using MI was not reported.

The Mangrove Recognition Index (MRI) (Zhang and Tian, 2013) was also developed for mangrove forest observation from space using multitemporal Landsat TM images with different tide levels. Changes in the low tide and high tide conditions can result to variations in the spectral signature of mangrove vegetation (Zhang et al., 2017; Lin and Fu, 1995). MRI index considers these intertidal effects and is sensitive to the wetness, greenness, and change of greenness (Table 1). In the equation, the Green Vegetation Index (GVI) expresses the vegetation characteristics while the Wetness Index (WI) expresses canopy water information. GVI and WI are products of tasselled cap transformation which is an orthogonal transformation of the original remotely sensed data space to a new feature space. Limited test of this index in Beilunhekou National Reserve Area of China using TM data have demonstrated that MRI can effectively separate mangroves from non-mangrove forests with 93.19% user's accuracy. The $|GVI_L - GVI_H|$ equation in the MRI formula generates higher values for mangrove vegetation due to the intertidal inundation in the coastal environment. Meanwhile, the sum of $|WI_L + WI_H|$ is high for mangrove forests and low for non-mangrove vegetation. Larger MRI values indicate that the pixels correspond to mangrove cover while lower MRIs correspond to other land cover such as terrestrial vegetation, water and bare soil. The applicability of MRI to other mangrove areas is then limited by the availability of tidal data, as tide condition vary significantly within regions and across the globe. Site-specific moisture and vegetation information during the low and high tides are necessary but might be limited from remotely-sensed images. To address this limitation, a Combine Mangrove Recognition Index (CMRI) was proposed by Gupta et al., 2018. CMRI (Table 1) utilizes NDVI to express the presence of vegetation and normalized difference water index (NDWI) to express water information of mangroves without the need for specific tidal data. Since NDVI and NDWI are negatively correlated, subtracting these indices increases the upper and lower range of the CMRI output and further magnifying the distinct values of different land covers with almost similar spectral signatures. CMRI was then used as an input to a classification method done to separate the Landsat scenes into four classes: water, land, non-mangrove vegetation and mangroves. The CMRI-based method requires training data to generate the output maps. The authors compared the result from the CMRI-based classification with that of NDVI, SAVI, and Simple Ratio (SR) wherein better accuracy (73.43%) was obtained by using the proposed index. Aside from Landsat, a new Sentinel-2 based index called the Mangrove Forest Index (MFI) was proposed by Jia et al., 2019. The index utilizes the reflectance of red-edge bands of Sentinel-2 imagery which are sensitive to submerged mangrove forests. The results showed that the submerged mangrove forests could be separated from the water background in the MFI output image. The study emphasized the capability of the NIR and red-edge bands in discriminating between vegetation and water. The said index was designed based on the reflectance peak in the NIR spectral regions of green vegetation (Jia et al., 2019).

Hyperspectral imageries are also being used for mangrove mapping (Kamal and Phinn, 2011; Jusoff, 2006). The Mangrove Probability Vegetation Index (MPVI) was proposed by Kumar et al. (2019) using bands derived from EO-1 Hyperion data. The Hyperion is a space-borne hyperspectral sensor acquiring 70 bands in the VNIR sensor and 172 bands in the SWIR, providing a total of 242 wavebands with ~10 nm bandwidth, and 30-m ground resolution (Green et al., 2003). The MPVI identifies the Hyperion image pixels corresponding to mangroves by calculating their correlation coefficients with a candidate mangrove spectrum (Table 1). Aside from MPVI, the same authors have also proposed the Normalized Difference Wetland Vegetation Index (NDWVI) using Hyperion bands: one SWIR band and one green band to discriminate mangrove from non-mangrove vegetation. Combination of different classifiers were used to identify the hyperspectral image data into mangroves and non-mangroves classes. Using MPVI alone

Table 1
Existing mangrove mapping indices for separating mangroves from non-mangrove pixels. The band inputs and ratio differ between the indices and satellite image used. Most of the earlier indices were implemented using Landsat images.

Index Name	Author	Formula	Satellite Image Used
Mangrove Index (MI)	Winarso et al., 2014	$MI = (NIR - SWIR/NIR \times SWIR) \times 10000$	Landsat
Mangrove Recognition Index (MRI)	Zhang and Tian, 2013	$MRI = \lvert GVI_L - GVI_H \rvert \times GVI_L \times (WI_L + WI_H)$ *where GVI - Green vegetation index; WI - Wetness index; Subscript L - at low tide; Subscript H - at high tide*	Landsat
Combine Mangrove Recognition Index (CMRI)	Gupta et al., 2018	$NDVI - NDWI$ *where NDVI is the Normalized Difference Vegetation Index and NDWI is the Normalized Difference Water Index*	Landsat
Mangrove Probability Vegetation Index (MPVI)	Kumar et al., 2019	$MPVI = \frac{n\sum_{n=1}^{n} R_i r_i - \sum_{n=1}^{n} R_i \sum_{n=1}^{n} r_i}{\sqrt{n\sum_{n=1}^{n} R_i^2 - \left(\sum_{n=1}^{n} R\right)^2}\sqrt{n\sum_{n=1}^{n} r_i^2 - \left(\sum_{n=1}^{n} r_i^2\right)^2}}$ *where n = total number of bands in the image, Ri is the reflectance value at band i for a pixel of the reflectance image, and ri is the reflectance value at band i for candidate spectrum of mangrove forest.*	EO-1 Hyperion
Normalized Difference Wetland Vegetation Index (NDWVI)	Kumar et al., 2019	$NDWVI = (R_{2203} - R_{559})/(R_{2203} + R_{559})$	EO-1 Hyperion
Mangrove Forest Index (MFI)	Jia et al, 2019	$MFI = [(\rho_{\lambda.1} - \rho_{B\lambda.1}) + (\rho_{\lambda.2} - \rho_{B\lambda.2}) + (\rho_{\lambda.3} - \rho_{B\lambda.3}) + (\rho_{\lambda.4} - \rho_{B\lambda.4})]/4$ *where the ρ_{λ} is the reflectance of the band center of λ, and i ranged from 1 to 4; λ1, λ2, λ3, λ4 are the center wavelengths at 705, 740, 783 and 865 nm, respectively.*	Sentinel-2

generated an overall accuracy of 73.98% while MPVI and NDWVI combined gave a higher accuracy of 85.01% (Kumar et al., 2019).

The previous mangrove indices reported different accuracy and advantages over the other. Mapping using MRI and MPVI still requires access to tide data and hyperspectral imageries, respectively, which may be a challenge in rapidly mapping mangroves in local and regional scales using free satellite imageries. The application of MI is more straightforward, but accuracy must still be explored including the application of the index to other satellite data such as Sentinel-2. The MFI was already tested for Sentinel-2 imagery using four spectral bands. The effectiveness of MFI was mainly validated between submerged mangrove forest and water, while its performance in discriminating mangrove from terrestrial forests was not yet examined. In the proposed MVI, the mangrove class will be discriminated against all land-use and land-cover present in a single tide Sentinel-2 image. NIR and SWIR are the commonly used bands among the previous indices. NIR band is an input to the MI and CMRI through the computation of NDVI. The ability of SWIR and green bands in delineating mangroves using the Hyperion-based MPVI was further explored through MVI, but the focus is shifted on the use of multispectral band spectral responses between mangroves and non-mangrove vegetation cover.

This study proposed a new simplified mangrove index, the Mangrove Vegetation Index (MVI) using the NIR, SWIR1 and green bands of Sentinel-2 to allow rapid and accurate mapping of mangroves without the need for complex classification techniques which maybe time-consuming and user-skill-biased. The index was designed by analysing the spectral signatures and characteristics of mangroves and non-mangroves datasets from different study sites in the Philippines and Japan. The index was formulated to capture the distinctive greenness and moisture content of mangrove pixels, discriminating them from non-mangroves and other non-vegetation cover such as bare soil, water, and built-up. The study then utilized MVI for nationwide mangrove mapping, and for mapping mangroves within and outside the Southeast Asia region. The MVI threshold were analyzed among land-cover and land-uses MVI values, and accuracy were computed using nationwide field-acquired mangrove inventory and drone data. MVI was then tested to Landsat bands having the same input bands (SWIR1, NIR and green) to determine the applicability and universality of the proposed index. Lastly, MVI-based mangrove mapping was automated using two platforms: an IDL-based MVI mapper for offline processing and Google Earth Engine (GEE) interface for rapid, accurate and large-scale mangrove extent mapping.

2. Data and methods

The first part of the methodology focuses on establishing the mangrove vegetation index by analyzing the varying spectral response of Sentinel-2 bands between the mangroves and non-mangrove pixels. The mangrove vegetation indices previously discussed were used as guide data for the analysis. Different combinations of the significant bands were tested, but this paper will focus on how the MVI was formulated. The MVI was then applied to Sentinel-2 imageries covering the selected mangrove sites (Fig. 1). The MVI accuracy was assessed for each study site using field surveys and high-resolution orthophotos. The second part of the methodology includes the generation of mangrove extent maps for the whole Philippines using the cloud-based MVI mapper. The generation of two automated tools for MVI mapping will be discussed.

2.1. Study sites

Five major mangrove sites in the Philippines and one in Japan were selected as the study sites, namely (1) Coron-Busuanga, Palawan; (2) Puerto Princesa, Palawan; (3) Panay Island; (4) Eastern Samar Island; (5) Zambales-Bataan and (6) Fukido, Ishigaki, Japan. A total of twelve subsites within the major mangrove sites were chosen for output validation (Table 2). Palawan is an archipelagic province located in the central western part of the Philippines. The island trends northeast-southwest between the South China and Sulu seas. Palawan is the Philippines' 'last ecological frontier' housing a huge collection of unique and diverse fauna and flora (Sandalo and Baltazar, 1997) including a total of 56,660 ha of mangroves (Long and Giri, 2011). It consists of 23 municipalities including Coron and Busuanga; and one city, Puerto Princesa. Coron comprises the eastern half of Busuanga Island, all of Coron Island and about 50 other minor islets. Meanwhile, Busuanga covers the western one-third of Busuanga Island, as well as Calauit Island, which both are part of the Calamian Islands. Both sites have rich natural mangrove forests where two Marine Protected Areas (MPA) were declared: the Sagrada-Bogtong Marine Reserve in Busuanga and the Decalve Strict Protection Zone (Bintuan-Sangat Marine Park) in Coron (Garces et al., 2012). Puerto Princesa is a city in the province of

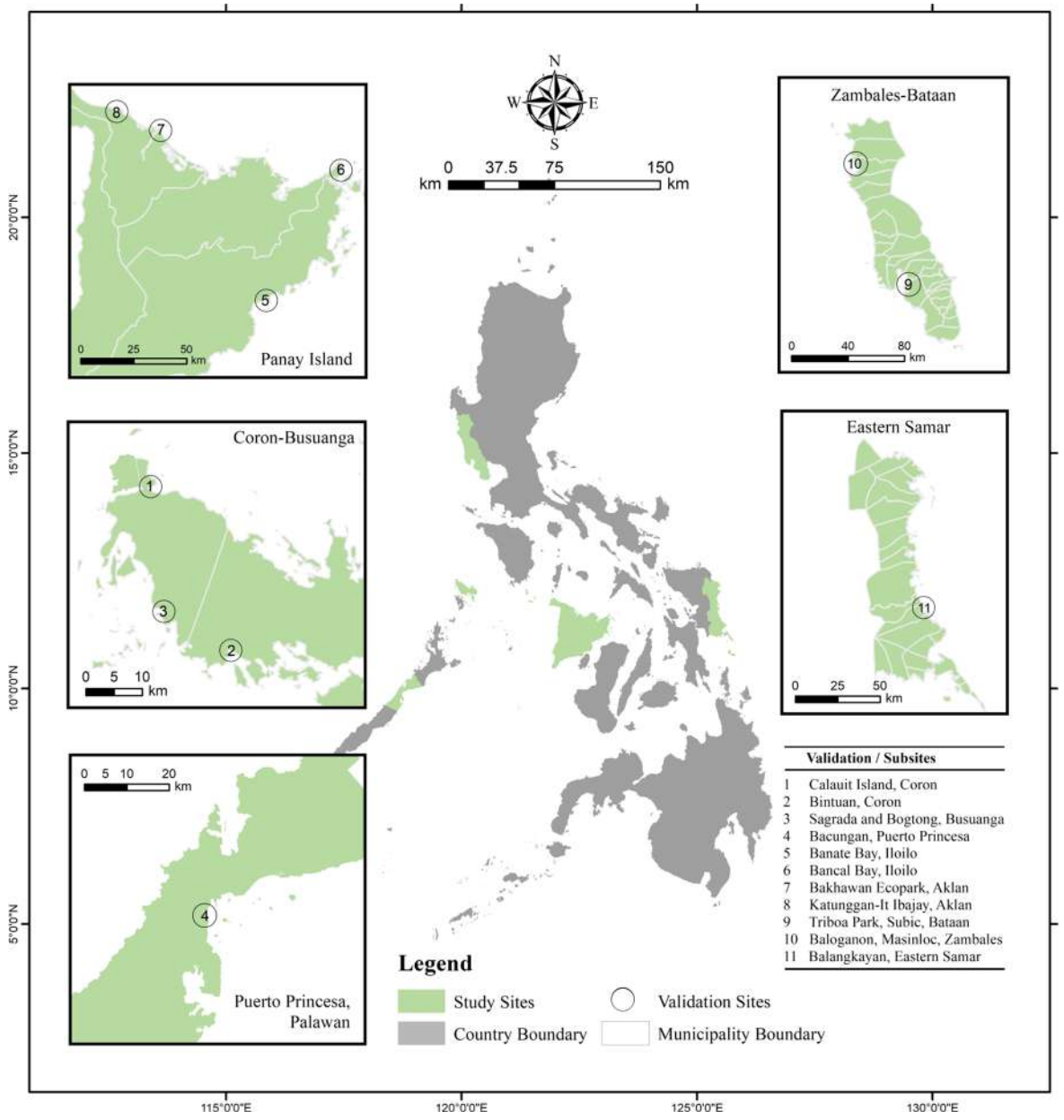

Fig. 1. Location of the major mangrove study sites (green) and the subsites in the Philippines where field data were collected. Coron- Busuanga, Puerto Princesa and Zambales-Bataan are located in Luzon, while Panay and Eastern Samar are in Visayas.

Table 2
Date of field survey collection and the corresponding Sentinel-2 data used for each mangrove study sites and subsites.

Study Sites	Coverage of Validation Data	Sentinel-2 Acquisition Date	Drone Survey/Field Inventory Date
Coron-Busuanga	Calauit Island	February 2017, 2018	July 2018
	Bintuan in Coron	February 2018	May 2018
	Sagrada and Bogtong in Busuanga	February 2018	May 2018
Puerto Princesa, Palawan	Bacungan	May 2018	October 2018
Panay Island	Banate Bay, Iloilo	August 2017	January 2018
	Bancal Bay, Iloilo	May 2019	January 2018
	Katunggan-It Ibajay, Aklan	February 2018	September 2018
	Bakhawan Ecopark, Aklan	August 2017	September 2018 / November 2017
Zambales-Bataan	Triboa Mangrove Park, Subic in Bataan	March 2018	August 2018
	Baloganon, Masinloc in Zambales	February 2016	November 2015
Eastern Samar	Balangkayan	June 2018	June 2019
Fukido, Ishigaki	Fukido Mangrove Park	February 2018	August 2018

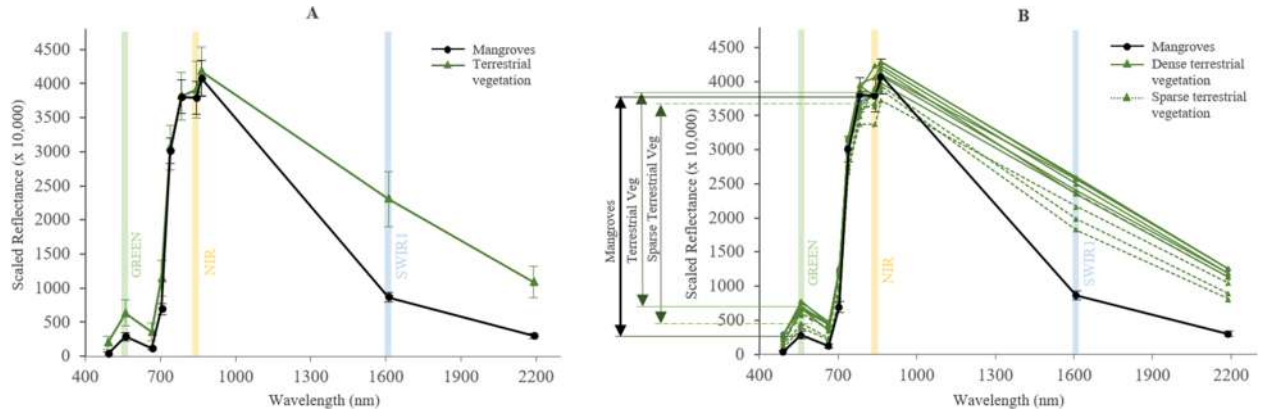

Fig. 2. Baseline theory based on the scaled spectral reflectance of mangroves and terrestrial vegetation (A) and mangroves, sample dense terrestrial vegetation and sparse terrestrial vegetation (B). The comparison focused on the reflectance values within the green (560 nm), NIR (842 nm) and SWIR1 (1,610 nm) of the Sentinel-2 image, where lower reflectance values of mangroves in the green and SWIR regions were observed compared to reflectance values of either dense or sparse vegetation. The reflectance in the NIR regions varies, but the difference of the reflectance values between the NIR and green regions in the terrestrial vegetation is always smaller than the difference observed in mangroves.

Palawan, supporting 11.7% of the total mangroves in the island. There are 18 true and 20 associate mangrove species found in Puerto Princesa, mainly within the Honda Bay, Ulugan Bay, and Puerto Princesa Bay.

Panay Island is a triangular island located in the western part of the Visayas. It is divided into four provinces: Aklan, Antique, Capiz and Iloilo. Two known species-diverse mangrove ecoparks are found in Aklan in Northern Panay: the 45-hectare Katunggan-It Ibajay (KII) Ecopark and the 79-hectare Bakhawan Ecopark. In Iloilo, mangroves are dominantly distributed in the east coast of the municipality of Banate, facing the Banate Bay. Masinloc and Subic are the two subsites selected within Zambales and Bataan, two adjacent provinces in the island of Luzon. Masinloc is a costal municipality in the province of Zambales with a reported mangrove extent of 109 ha, 36% of which are old stands. Subic Bay Freeport Zone or Subic is a special economic zone covering portions of Olongapo City and the towns of Subic in Zambales and Morong and Hermosa in Bataan. It houses the Triboa Bay Mangrove Park, a two-hectare reforestation project.

Fukido Mangrove Park in Japan was added as an additional site for MVI validation. The Fukido Mangrove Park is located in the northeastern part of Ishigaki Island, southwest of Ryukyu Islands. This natural and estuary mangrove forest was designated as a national sanctuary by the Ministry of the Environment of Japan (Sharma et al., 2014). *Rhizophora stylosa* and *Bruguiera gymnorrhiza* are the only dominant species in the mangrove park.

2.2. Satellite data and pre-processing

The Sentinel-2 Multispectral Imager Instrument (MSI) Level 1-C images covering KII Ecopark, Coron, Busuanga and Fukido Mangrove Park were downloaded from Sentinel Scientific Data Hub (European Space Agency, 2018) (see Table 2). The product is already orthorectified, georeferenced, and radiometrically calibrated into top-of-atmosphere (ToA) reflectance data. Atmospheric correction was carried using Sen2Cor standalone tool, which can be processed alternatively in the S2A Toolbox of the Sentinel Application Platform (SNAP). This processor uses image-based retrievals with Look-Up tables (LUTs) precalculated from the libRadtran model to minimize or remove atmospheric effects from level 1-C images (Main-Knorn et al., 2015). All Level-2A bands were resampled to 10 m pixel size using SNAP (ver. 5.0) geometric operation tool.

Sentinel-2 images with the least cloud cover and at least close to the drone survey date were selected. A single Sentinel-2 tile may cover more than one subsite, such as the Path T50PRU covering Calauit, Bintuan and Sagrada-Bogtong in the Coron-Busuanga sites. Once resampled, the needed bands were stacked: from Blue (490 nm, Band 2), Green (560 nm, Band 3) to NIR (842 nm, Band 8), NIR Narrow (865 nm, Band 8A), SWIR1 (1610 nm, Band 11) and SWIR2 (2190 nm, Band 12). MVI can already separate the mangroves from clouds and non-mangrove vegetation based on the threshold test. Selection of cloud-free Sentinel-2 images can significantly hasten the mapping time using MVI due to less noise pixels to be removed in the final output.

Landsat-8 scenes with minimum cloud cover for year 2017 were also obtained for MVI comparison. The data was downloaded from the USGS Landsat 8 Surface Reflectance Tier 1 dataset in Google Earth Engine. This dataset is already atmospherically corrected surface reflectance using the LEDAPS software (Schmidt et al. 2013). The surface reflectance products have been atmospherically corrected using Land Surface Reflectance Code (LaSRC) algorithm which includes a cloud, shadow and water mask.

2.3. Formulation of MVI

2.3.1. Sentinel-2 input bands

Based on related studies on mangrove vegetation properties and spectral responses within the spectral wavelengths, three multispectral bands were selected to be formulated into the MVI. These are the SWIR1, NIR (Band 8) and green (Band 3). The SWIR and NIR bands were found to be effective in characterizing water absorption in vegetation, and vegetation greenness, respectively (Manna and Raychaudhuri, 2018; Wang et al., 2018). Both SWIR1 and SWIR2 are affected by leaf liquid water. SWIR1 region is more useful in extracting vegetation information such as nitrogen compared to SWIR2 (Herrmann et al., 2010). High nitrate concentration in plants was found to increase root water uptake (Górska et al., 2010), resulting to synergetic transport between nitrate and water (Tyerman et al., 2017). Although SWIR2 is useful for soil and vegetation unmixing, the spectral band needed to extract canopy moisture information for MVI must also be affected by the background soil moisture to help distinguish wet from dry vegetation. As seen in Figs. 2 and 3, the difference in the canopy moisture-affected surface reflectance of mangroves and terrestrial vegetation are more distinguishable in the SWIR1 region. Meanwhile, the green wavelength region was found to be optimal for species discrimination in addition to the water absorption regions (Kumar et al., 2019; Prasad and Gnanappazham, 2015). The three bands were stacked into one data file and were imported to ENVI where MVI formula was applied.

2.3.2. Development of MVI

The main test spectral bands in the formulation of the index was derived from the atmospherically corrected Sentinel-2 images acquired

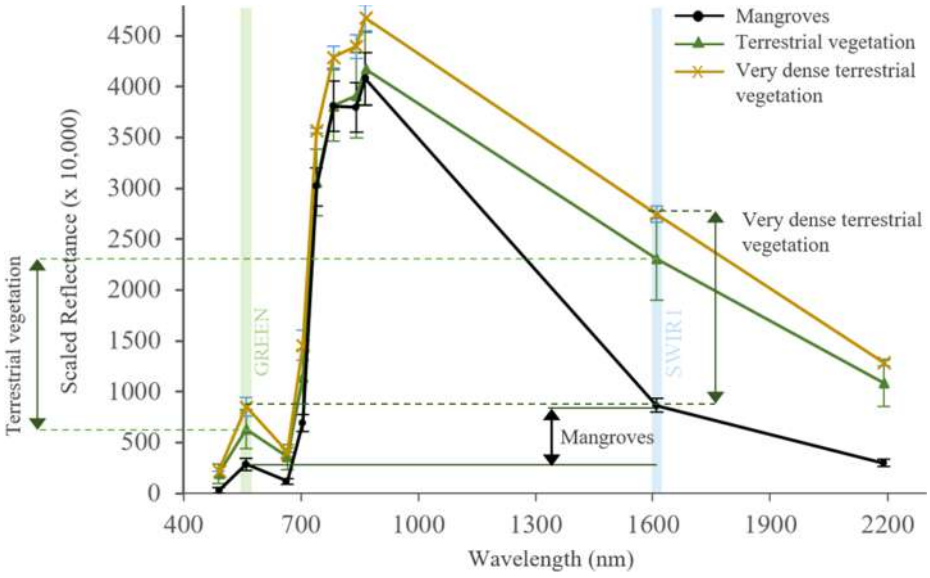

Fig. 3. Baseline theory based on the spectral reflectance of mangroves, terrestrial vegetation and very dense terrestrial vegetation, showing the extent of the reflectance differences between the SWIR1 and green regions of each class. The difference between the SWIR and green values for mangroves is relatively smaller than the difference observed in the same spectral regions of sparse to dense and very dense terrestrial vegetation. Very dense vegetation pixels commonly have high SWIR values, making it separable from the mangrove pixels.

over the Coron-Busuanga site. This is due to the occurrence of various land-cover and land uses such as thick mangroves, sparse mangroves, forests and other terrestrial vegetation classes, built-up surfaces, water and bare soil. One hundred training data for each mangroves and non-mangroves vegetation classes were collected and the equivalent reflectance values in the green, NIR and SWIR1 wavelengths were analyzed (Figs. 2 and 3). Vegetation types, either coastal or terrestrial, have higher reflected radiation in the NIR wavelengths than in visible wavelengths. Chlorophyll strongly absorbs visible light from 400 to 700 nm wavelength while cell structure of the leaves strongly reflects near-infrared light from 700 to 1100 μm wavelength. Leaf pigments and cellulose are transparent to the NIR wavelengths resulting to high leaf reflectance (Huete, 2004). Among the visible spectrum, reflectance is highest in the green wavelength (Ashraf et al., 2011; Rullan-Silva et al., 2013). Smaller difference in the reflectance values between the visible regions reflects that the forest is sparse, while larger difference reflects that the forest is dense. Between forest types, however, there are distinct differences observed in the reflectance levels in the NIR and green regions when mangrove forest and terrestrial forest were compared.

The NIR reflectance of terrestrial vegetation could be either higher or lower than mangroves (Fig. 2A). It is usually dependent on the health of the internal chlorophyll structure and leaf cellulose which reflect the near-infrared EM waves. Among the sample terrestrial vegetation data, lower reflectance in the green wavelength is observed when its reflectance in the NIR is lower, but not to the extent that it is lower than the green reflectance values of mangroves (Fig. 2B, 'sparse terrestrial vegetation'). Pixels selected within terrestrial forests classified as 'dense terrestrial vegetation' show high reflectance both in the NIR and the green regions of the spectrum. If we then subtract the green values from NIR, the difference will be always greater for mangroves compared to terrestrial vegetation classes.

In some cases, there are vegetation types including very dense trees within closed forests and wet dense grass with relatively higher NIR values than mangroves (Fig. 3) that may produce very small to negligible difference if only the first baseline theory (Fig. 2) will be considered. Thus, there is a need for additional observation to discriminate these types of vegetation from mangroves. It was observed that non-mangroves vegetation with high reflectance in the NIR wavelength also have higher SWIR values than those of mangroves (Fig. 3). If we then subtract the green values from SWIR, the difference will be always smaller for mangroves. The leaves and canopies of mangroves contains higher water content in comparison to most of the terrestrial vegetation (Kumar et al., 2019; Tomlinson, 1994). The reflectance of mangroves in the SWIR1 spectrum is also lower due to presence of moist soil as affected by tide inundation. This is clearly visible in Fig. 3 where the scaled reflectance values of mangroves is below 1000.

The two main observations were considered into the Mangrove Vegetation Index (MVI) equation:

$$MVI = (NIR - Green)/(SWIR1 - Green) \quad (1)$$

where NIR, Green, and SWIR1 are reflectance values in Sentinel-2's band 8, band 3, and band 11, respectively. The first part of the equation | NIR-Green | enhances the differences of vegetation greenness between mangrove forests and terrestrial vegetation; while the second part of the equation |SWIR1-Green| expresses the distinct moisture of mangroves due to its environment. MVI measured the probability of mangrove pixels by utilizing the green, NIR and SWIR1 bands to highlight mangroves' greenness and moisture, separating it from other classes especially from terrestrial vegetation. Higher quotient reflects higher probability of a pixel being a mangrove. Minimum and maximum MVI thresholds were set using sparse and dense mangrove data. Although the difference of red band and NIR is larger than the difference of the green band and NIR (Fig. 3), the gaps in the spectral signature of mangroves and terrestrial vegetation classes are larger and more distinguishable in the green region (SD = 286) than in the red region (SD = 153). The larger the spectral gap, the larger will be the difference in the MVI dividend between the mangrove and non-mangrove classes which will be useful in separating the mangroves.

2.3.3. MVI threshold

Training samples were selected from a Sentinel-2 image containing different land-use and land cover. Each of the training pixels represents pure sample of the selected class. The spectral signatures of the selected pixels were checked prior to MVI generation. Mean, upper and lower thresholds of mangroves and non-mangroves were identified by generating the MVI for the following classes: mangroves, terrestrial vegetation (forest and non-forest), bare soil, built-up, water and clouds.

2.4. Application of MVI to Sentinel-2 images

Atmospherically corrected Sentinel-2 images covering the six major sites were used as inputs for the index computation (Fig. 4). All bands were resampled to 10 m resolution and were stacked as one file. The MVI formula was applied to the stacked images using ENVI 5 band math tool. The MVI outputs were then filtered to select only the pixels within the mangrove MVI values based on the identified threshold value. Each

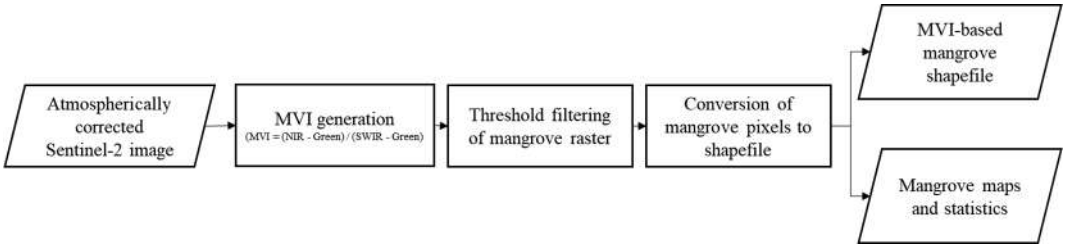

Fig. 4. Workflow used in generating the MVI-based mangrove maps from Sentinel-2 imagery. Atmospherically corrected image was used as inputs where the green, SWIR1 and NIR bands were utilized in generating the MVI output image in ENVI 5. Threshold selection is a significant step to separate the mangrove MVI pixels from the other classes. The filtered mangrove output was exported in ArcGIS software to facilitate noise pixels deletion, map layout and statistics computation.

filtered mangrove MVI raster covering the sites was converted into shapefile. Cleaning of noise pixels, if applicable, were applied by overlaying the shapefile to the false-color Sentinel-2 image.

2.5. Index accuracy assessment

A total of 2,727 validation pixels were used in the study from mangrove field inventory and high-resolution drone orthophotos as reference maps. The accuracy was computed by calculating the validation pixels that were correctly mapped in the MVI outputs. For a single subsite with both field inventory and drone data available, the mean accuracy between the two data was used.

Most of the field inventory data contain information on the mangrove tree location, the species name, and tree height. These mangroves were selected and GPS-tagged on site to collect representative tree sample for each species present, regardless of the zonation, vegetation density, and distance from the shore. For the purpose of the study, only the mangrove location is needed. Higher validation samples were obtained from Masinloc due to an existing plot-level field inventory data. The drone photos within the subsites were acquired using DJI Phantom 3, DJI Phantom 4, and Sensefly eBee drones mounted with either RGB or Sequoia multispectral camera. The generation of orthophotos was carried in Pix4D software. The spatial resolution of the orthophotos varies from 3 to 5 cm, high enough to be used as validation data.

2.6. Application to Landsat OLI

The bands needed to generate an MVI from Sentinel-2 imagery are also present in Landsat. Bands 3, 5, and 6 are the equivalent green, NIR and SWIR1 bands in Landsat-8, as seen in the formula below and in Table 4. Landsat SWIR1 (Band 6) was selected over SWIR2 (Band 7) to generate comparable results with Sentinel2-based MVI which also utilizes SWIR1 (Band 11). Both are within similar wavelength range, from 1565 nm to 1655 nm. The spectral wavelength comparison between the two sensors is shown in Table 4.

$$Landsat - 8\ MVI = (B5 - B3)/(B6 - B3) \quad (2)$$

$$Sentinel - 2\ MVI = (B8 - B3)/(B11 - B3) \quad (3)$$

The threshold for Landsat8-based MVI was identified using the atmospherically corrected Landsat image covering Calauit, Busuanga. Visual variations of the output MVI mangrove maps from the two satellite data were examined. In addition, correlation between Landsat and Sentinel MVI input bands were analyzed to understand the similarities or differences between the output MVIs.

2.7. Comparison with vegetation and biophysical indices

The correlation of MVI with NDVI, LAI and fractional vegetation cover (FVC) were examined. LAI and FVC were generated from the atmospherically corrected and resampled (10 m) Sentinel-2 data using the biophysical processor toolbox of SNAP. These products are outputs of tested, generic algorithms based on specific radiative transfer models. The generation of LAI and FVC were composed of three main steps: (1) normalization of the inputs, (2) implementation of the artificial neural network (ANN) algorithm, (3) denormalization of the output and (4) generation of quality indicator (Weiss and Baret, 2016). The comparison and analysis of MVI with LAI and FVC were employed using mangrove pixels obtained from two forest types with different greenness and moisture characteristics: riverine and fringe mangrove forests. Index correlation and map comparison were done. The efficiency of MVI in determining mangrove health was tested by comparing it with the NDVI, LAI and FVC values within the two forest types. In addition, Sentinel-2 derived chlorophyll-a (C_a) and canopy water (C_w) were generated from SNAP to determine their correlation with MVI. The C_a and C_w are two readily available Sentinel-2 biophysical products for canopy greenness and canopy moisture analyses.

2.8. Automation of MVI

To facilitate faster processing especially for large-extent mangrove mapping, a sub-automated workflow and an automated workflow were designed which can be respectively implemented offline and online. The first one is an IDL-based 'MVI Mapper' tool which was developed for offline semi-automated processing. For fully automated processing online, the MVI Mapper was also implemented in Google Earth Engine.

2.8.1. IDL-based offline MVI processing

The *IDL,* short for Interactive Data Language, is a program language widely used in astrophysics which is mainly for data analysis and visualizations of complex numerical data. IDL consists of both an interactive programming environment and a programming language, its main advantage over other languages (Bowman, 2004). Since IDL is a commercial software, the IDL used in the study is the version included in the ENVI 5 package (IDL v. 8.5). The MVI script is called the 'MVI Mapper' which was developed as guided by the initial workflow (Fig. 4). The non-automated component includes the downloading of Sentinel-2 image from either Earth Explorer or Sentinel Scientific Data Hub, and atmospheric correction and resampling in SNAP software. The automated MVI script facilitates the processes of MVI image generation, image masking using the user-selected threshold, and generation of MVI vegetation raster, mangrove raster and mangrove shapefile.

The MVI mapper will initially require users to input the directory of the resampled atmospherically corrected data and the desired output folder directory. The mapper will then proceed to the generation of MVI images based on the inputted threshold. Total time of processing for the selected sites were recorded. The IDL based methodology were mainly utilized if the satellite data were already pre-downloaded or available. It can be used in any computers with an IDL software installed, without the need for internet connection as the IDL workflow runs offline. In the case of the nationwide mangrove mapping, the IDL based method will still consume some time for data download.

2.8.2. Google Earth Engine-based MVI mapping

An online MVI mapper was developed for larger extent mangrove

mapping where manual satellite download and pre-processing is not needed. The workflow is fully automated, from the sourcing of atmospherically corrected Sentinel-2 (Level-2A) input from Google Earth image database to the generation of four products: RGB and false color composite images, MVI vegetation raster and MVI mangrove raster. A graphical user interface (GUI) was further developed for user-friendly processing. The MVI mapper requires users to input the desired Sentinel-2 tile, the start and end date, the lower and higher MVI mangrove threshold, and the selected outputs from a list of products, including RGB and false color composite images, MVI vegetation raster and MVI mangrove raster. False color composite and RGB images were included as outputs to aid in the quality assessment of the generated mangrove raster. The conversion of MVI raster to shapefile is done outside the GEE where data cleaning is possible.

2.9. Generation of nationwide MVI-based mangrove maps

The MVI was initially applied to the six study sites consist of twelve subsites, eleven of which are in the Philippines. The GEE-based MVI Mapper was utilized to generate an updated nationwide mangrove maps using Sentinel-2 images acquired within year 2019. Available 2016 mangrove map from Global Mangrove Watch was used to determine the needed Sentinel-2 tiles to be included in the processing. A total of 106 tiles were detected. The mangrove MVI raster outputs were downloaded and quality-checked in ENVI software. The raster images were converted to shapefiles in ArcGIS. In some images with noise pixels, false color composite images were overlaid to aid in data cleaning. The total area of mangroves per tile was computed, which was further used in calculating the current mangrove extent in the country.

2.10. Generation of MVI for selected countries in Southeast Asia

The MVI was initially tested in a Sentinel-2 image covering Ishigaki, Japan as one of the study sites. The IDL-based MVI Mapper was also applied in generating the mangrove maps of other selected countries including Indonesia, Cambodia, Thailand, and Vietnam. The purpose of this is to test the applicability of MVI in mapping mangroves in different mangrove forest types and mangrove zones. For each country, the false color image composite was used to determine the specific Sentinel-2 tiles with mangrove cover. The map outputs for the said countries were compared with previous mangrove extent estimates.

2.11. Application to mangrove forests outside Asia

Three additional mangrove sites were added to test the applicability of the MVI for mapping mangroves outside Asia. The mapping threshold, greenness and moisture characteristics were compared between mangrove forests. These sites are Baía de São José, Amazon Coast in Brazil, Mabokweni in Tazania, and Prince Regent National Park in Western Australia. These are representatives of mangrove forests located in three different continents: South America, Africa, and Australia, respectively, with varying substrates, mangrove types, and mangrove ecosystem characteristics.

2.12. Index uncertainties due to tidal level and rainfall

Three subsites were selected to determine the effect of tidal level and precipitation to the MVI metrics, including mangrove area and mean mangrove MVI value. These are Bintuan in Coron, Sagrada in Busuanga, and Pilar in Siargao. The Coron and Busuanga sites are located in the western region of the country with West Philippine Sea to the west and Sulu Sea to the southeast. The Siargao site was selected to represent an area located in the eastern region, facing the Pacific Ocean to the east. Sentinel-2 images acquired within different months and season of 2019 and early 2020 were used for this section. For Coron and Busuanga, the data downloaded were acquired January 8, 2019 (dry season); June 12, 2019 (wet season); December 29, 2019 (end of wet season); and January 23, 2020 (dry season). For Siargao, the data were acquired February 21, 2019 and August 10, 2019 for the dry and wet season, respectively.

Mangrove area and mean mangrove MVI value were computed for each satellite data based on the optimal minimum MVI threshold needed to separate the mangroves. The variation in the MVI products were explored through comparison with precipitation and tidal data which may exhibit monthly and seasonal changes. The tidal data was acquired from WXTide32 Version 4.7 software (Hopper, 2007) specifically for 10:20 AM timestamp to be similar with the time of satellite acquisition. The tide stations used are Coron, Busuanga Island located 120°12.00 'E, 12°1.00 'N, and Pilar, Siargao located 120°6.00 'E, 9°52.00 'N. The default offset values for tide height measurement from the selected reference stations were used. The daily precipitation data was acquired from NOAA National Centers for Environmental Prediction (NCEP) Climate Forecast System Reanalysis dataset (CSFR) with 19.2-km grid resolution downloaded from https://app.climateengine.org/climateEngine. The total precipitation on the day of satellite acquisition and on three days earlier was included as one of the meteorological metrics. Moreover, the mean values of FVC, C_w, NIR, and SWIR within the mapped mangrove areas were computed to better understand the MVI results. FVC and C_w were generated using the same methodology discussed in Section 2.7.

3. Results and discussion

3.1. Mangrove vegetation index

The proposed MVI utilized three spectral bands, namely, SWIR1, NIR, and green, or bands 11, 8 and 3, respectively, in the case of Sentinel-2 (Eq. (1)). The SWIR band is commonly used in characterizing water absorption characteristics in vegetation (Manna and Raychaudhuri, 2018). It was observed by Winarso et al. (2014) as an effective band in their mangrove index (MI) where it expresses the absorption of electromagnetic wave as affected by tidal-caused wet soil. SWIR bands were said to be significant for mangrove extent classification, then followed by the NIR band (Wang et al., 2018). NIR was selected as target input band due to its ability to express vegetation greenness. It was reported to be the spectral region where mangroves recorded the highest reflectance in sample hyperspectral images (Basheer et al., 2019). Reflectance of mangroves also differs among the bands in the visible region, although the difference in the spectral curve between most mangrove species are reported to be small (Kamaruzaman and Kasawani, 2007). The reflectance is lower in both the blue and the red regions of the spectrum due to its absorption by chlorophyll for photosynthesis (Figs. 2 and 3). Combinations of SWIR1, NIR and green bands resulted to the MVI.

The proposed index is the first mangrove index to utilize green, NIR, and SWIR1 in a single equation, in contrast with the derived NDVI and NDWI indices used in generating CMRI (Gupta et al., 2018). With these bands, the MVI formula reflected two main properties of mangrove vegetation: greenness and moisture. MVI allows the calculation of ratio between the greenness and moisture resulting to values distinct to mangrove classes. Fig. 3 have shown that the MVI values can already discriminate mangrove from non-mangroves vegetation, regardless of the density of terrestrial vegetation cover. In comparison with NDVI, LAI and other vegetation indices, MVI values are high for mangrove vegetation only and thus can be utilized as a single input for index-based mangrove mapping. Previous works reported the need to still combine the common vegetation indices such as NDVI, SR and SAVI to obtain higher accuracy in mangroves (Alsaaideh et al., 2013; Kongwongjan, et al, 2012).

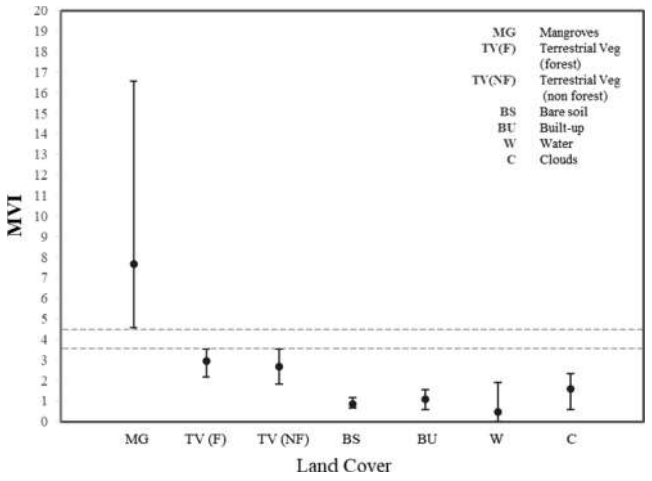

Fig. 5. Mean, maximum and minimum MVI values of mangroves and non-mangroves classes: terrestrial vegetation-forest (TVF), terrestrial vegetation-non forest (TVNF), bare soil (BS), built-up (BU), water (W) and clouds (C). The minimum threshold for mangrove MVI was observed to be 4.5, higher than the maximum MVI values of terrestrial vegetation (3.5). Clouds, water, built-up and bare soil generated lower MVI values than the vegetation classes due to differences of spectral reflectance in the green, NIR and SWIR bands. The lowest MVI was recorded for water due to its high absorption in the three spectral regions used for MVI.

3.2. MVI threshold

The MVI values of pixels identified as mangroves, terrestrial vegetation (forest and non-forest), bare soil, built-up, water and clouds were plotted in Fig. 5. A total of 50 pure training samples were collected for each land cover class. For mangroves, training samples were chosen to represent all types of pure mangroves, ranging from sparse to dense cover, and from fringe to riverine mangrove forests. The mean mangrove MVI values is 7.7, with maximum value of 16.5 and minimum value of 4.5. The whole extent of this threshold is separated from the threshold of terrestrial forest and non-forest vegetation, with maximum threshold up to 3.6 only. This is the result of the distinct spectral response of mangroves in the green, NIR and SWIR1 wavelengths. To generate higher MVI values, the dividend (NIR-green) must be large while the divisor (SWIR-green) must be small. In terms of terrestrial vegetation, its reflectance in the NIR region could be higher than mangroves but subtracting its reflectance values in the green region from that of NIR made the MVI dividend smaller.

The SWIR1 values of terrestrial vegetation is also higher than mangroves, while the SWIR1 values of mangroves is usually low due to incident radiation absorption by leaf water. The SWIR1 and NIR values of terrestrial forest is lower than the terrestrial non-forest vegetation (Fig. 6). MVI, similar with other mangrove indices, is well dependent on the moisture information of mangrove pixels as affected by its coastal habitat (Zhang and Tian, 2013). The proposed index assumes that coastal wetland conditions can already be reflected by the SWIR1 values, mainly due to the leaf water content (Huete, 2004) and background reflectance of soil and water. Canopy water content of mangroves increases with increased salinity (Nguyen et al., 2017) and high humidity levels because of tidal inundations (Al-Saidi et al., 2009), factors that are common in a mangrove environment. Some uncertainties in this assumption will be discussed later in Section 3.12.

The MVI values of bare soil and built-up ranges from 0.65 to 1.15 and 0.6 to 1.57, respectively (Fig. 5). Soil (BS) and built-up (BU) both have high reflectance values within the NIR and SWIR1 regions (Fig. 8). The SWIR1 reflectance of soil is highly dependent on the mineral, organic matter and water content at the surface (Cierniewski and Kuśnierek, 2010; Huete, 2004). High reflectance of built-up in SWIR1 region is mainly driven by urban surfaces and man-made materials. With high NIR and low green reflectance values, the MVI formula dividends for soil and built-up classes are high. However, the MVI divisor is also high due to high reflectance in the SWIR1 region, to be subtracted by low reflectance values in the green region. The resulting MVI values are relatively lower than mangroves MVI, as shown in Fig. 5. The reflectance of water (W) is low in all spectral regions especially in the NIR (Fig. 6) due to its high absorbing properties.

The 4.5 threshold for extracting mangrove pixels was applicable to the eleven subsites used in this study. In the case of small mangroves located in drier locations such as the Triboa site (2 ha), the threshold was adjusted to a lower value of 3.5. The said threshold can already separate the mangroves from the terrestrial vegetation, which also have lower MVI values in Triboa compared to the terrestrial vegetation within the other sites. It was previously observed that the SWIR1 value of mangroves increases as the leaf water content decreases (Huete, 2004; Tucker, 1980), which can lessen the output MVI values. The reflectance of mangrove in the visible regions, on the other hand, is not responsive to the factors affecting canopy moisture such as tidal inundation (Huete, 2004).

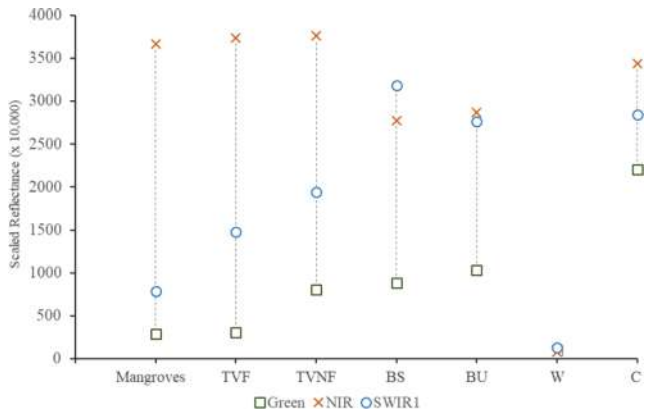

Fig. 6. Scaled reflectance values of mangroves, terrestrial vegetation-forest (TVF), terrestrial vegetation-non forest (TVNF), bare soil (BS), built-up (BU), water (W) and clouds (C) in the green (560 nm), NIR (842 nm) and SWIR1 (1,610 nm) regions. By disregarding the water class, the lowest green and SWIR1 reflectance values were obtained with mangroves, while the terrestrial vegetation classes registered higher green values than mangroves.

3.3. Generated MVI images

Sentinel-2 images covering the six study sites (Table 3) were used in generating the MVI bands. Comparison of the false color composites and the MVI products for the Philippine sites are shown in Figs. 7–9. Clear delineation of mangroves was observed especially in Busuanga (Fig. 8), Coron (Fig. 9-A) and Calauit Island (Fig. 9-B) where large mangrove covers exist.

Dense terrestrial vegetation situated in the northern part of Coron and Calauit generated lower MVI values, discriminating it from the mangroves. Most of these vegetation areas are located within dense closed forests. Inland water was successfully separated from the mangrove cover in sites including Calauit Island (Fig. 9-B), Bacungan, Puerto Princesa, Palawan (Fig. 9-C), and Bakhawan Ecopark, Aklan (Fig. 7-A), although some water pixels were already masked out in the pre-processing steps. Some of these inland water areas were reported to be misclassified as 'mangroves' in previous mapping works (Bunting et al., 2018; Long and Giri, 2011). This was observed when the MVI-based map and the Global Mangrove Watch data of Calauit Island were compared, with only the earlier delineated the inland water from the actual mangrove cover, with water MVI values lower than 4. The Global Mangrove Watch (GMW) utilized mangrove masks based on the mask data of Giri et al. (2011) and Spalding et al. (2010) while the water occurrence layer was sourced from Pekel et al. (2016). Pekel's water

Table 3
Source of validation data and total number of validation pixels for the twelve subsites to assess the accuracy of the generated MVI maps. Geotagged mangrove location from field inventory and randomized points selected within the drone-acquired orthophotos were the main validation data used in this study. The overall accuracy was then computed from the average accuracy of the subsites.

Study Site	Coverage of Validation Data	Validation Data	Total Validation Pixels
Coron-Busuanga	Calauit Island	Drone orthophoto	50
	Bintuan (Coron)	Drone orthophoto	50
	Sagrada and Bogtong (Busuanga)	Drone orthophoto	50
Puerto Princesa, Palawan	Bacungan	Drone orthophoto	50
Panay Island	Banate Bay, Iloilo	Drone orthophoto	50
	Bancal Bay, Iloilo	Drone orthophoto	50
	Katunggan-It Ibajay, Aklan	Drone orthophoto	50
	Bakhawan Ecopark, Aklan	Drone orthophoto and field inventory data	90
Zambales	Triboa Mangrove Park, Subic	Drone orthophoto	15
	Baloganon, Masinloc	Field inventory data	2,148
Eastern Samar	Balangkayan	Drone orthophoto	50
Fukido, Ishigaki	Fukido Mangrove Park	Drone orthophoto and field inventory data	74

masks used by GMW has a spatial resolution of 30 m while the initial water mask used in this study is 10 m as derived from the resampled Sentinel-2 images. Since mangrove forests are located near the shoreline and therefore periodically submerged by tides, distinction between mangrove and water pixels could be affected by the time of satellite acquisition. Discriminating submerged mangrove from water background was previously performed using an index dependent on the reflectance peak in the NIR spectral regions (Jia et al., 2019), while the proposed MVI relies on the coupling responses of NIR and SWIR1 with the green wavelength among vegetation and water pixels. Other indices utilize NDWI as an input to separate water classes (Gupta et al, 2018). Thin mangrove forests such as those located in Banate Bay, Iloilo, (Fig. 7-C) and Masinloc, Zambales (Fig. 7-E) were correctly mapped using MVI. Sentinel-2 10 m spatial resolution allows finer delineation of these mangroves near the coastline and along the river delta. Small patches of mangrove can still be detected, which is inadequate when a coarser satellite such as Landsat is used (Hoa and Binh, 2016). To consider the accuracy in delineating patches of mangroves, some of the validation points were selected from small and sparse cover.

The Japan study site is the Fukido Mangrove Park in Ishigaki Island. This site is relatively smaller than the Philippines sites, with two dominant species namely, *Rhizophora stylosa* and *Bruguiera gymnorrhiza*. The total mangrove area estimated using MVI for the entire Ishigaki Island is 87 ha. This is close to the previously estimated area of 80 ha (Alsaaideh et al., 2013) and 100 ha (Ministry of Environment Reference Map). The drone and mangrove inventory both gave an accuracy of 92%.

3.4. Index accuracy

Selected mangrove drone orthophotos used in validating the accuracy of the MVI maps are shown in Fig. 10. These orthophotos have a spatial resolution of 3 to 5 cm. Multiples flights were conducted in areas with more than one subsite.

The overall accuracy of MVI-derived mangrove maps as validated by high resolution drone orthophotos and field inventory data is 92% (Table 5). Ninety-four to 100% accuracy was computed for the Palawan sites: Calauit, Coron, Busuanga and Bacungan in Puerto Princesa. In Busuanga, the MVI perfectly mapped the whole mangrove extent with an accuracy of 100%. These sites are the relatively larger study sites with both sparse to dense mangrove cover. The physiographical classification of mangroves in Palawan falls under two major forest types, the fringe and riverine (Dangan-Galon et al., 2016). The validation site locations in Coron and Busuanga are within fringe mangroves, while the Calauit site is within both fringe and riverine forests. The result implies the capability of MVI to map mangroves regardless of the distance from the shore which causes variations in water salinity, tide inundation and species composition.

The index accuracy is also high for the two Iloilo sites: Banate Bay (90%) and Bancal Bay (98%). These are fringe mangroves along the bays, situated between other coastal features and the inward terrestrial vegetation. Lower accuracies were computed from the smaller mangrove sites, including KII Ecopark, Aklan (80%), Balangkayan, Samar (80%) and Triboa Mangrove Park (87%). The KII Ecopark is 45 ha while Triboa is only around two hectares. The accuracy within the said sites are seen to be affected by the spatial resolution of the input Sentinel-2 image which is in 10 m resolution, while the drone data is at few centimeters. Some of the validation points are located within Sentinel-2 mixed pixels, which can only be separated in the higher resolution validation data. Lower accuracy in KII Ecopark could also be influenced by the tide level during the satellite acquisition as a large area of the forest is exposed during low tide.

Meanwhile, few mixed pixels consisting of healthy and damaged/dead mangroves in the Balangkayan site could have lessen the MVI accuracy. Pure 'damaged to dead mangrove pixels' have lower reflectance in the NIR region and higher in the green, so the resulting MVI is lower. The decrease in NIR reflectance is caused by the absence of healthy leaf tissues, while the increase in green is driven by the inability of stressed vegetation to absorb visible light (Kovacs et al., 2001). Samples of the pure dead mangroves pixels in Balangkayan have MVI values ranging from 0.9 to 1.5, while mixed healthy and dead mangroves pixels have an MVI ranging from 1.9 to 4.6, depending on the ratio of the dead and alive mangroves per Sentinel-2 pixel. All pure mangrove pixels have an MVI values higher than 4.5.

3.5. Application to Landsat data

Prior to MVI comparison between Sentinel-2 and Landsat data, the agreement between the input bands were determined first by obtaining sample reflectance values in the green, NIR and SWIR1 regions. Three land cover classes (Fig. 11) were included in the analysis: mangroves, non-mangrove vegetation such as forest and grass, and non-vegetation which includes built-up and bare soil.

Results show that the green, NIR and SWIR1 bands of the input Landsat and Sentinel bands have overall good spectral fit with R^2 values between 0.42 and 0.92. The highest linear fit was obtained from the non-mangrove vegetation samples as observed in all three bands (R^2 = 0.80 to 0.92). In mangroves, moderate agreement was obtained in the green (R^2 = 0.42) and NIR region (R^2 = 0.60), but high in the SWIR1 region (R^2 = 80). This implies that we can expect some degree of differences in the output Landsat-based and Sentinel-based MVI images. Low spectral fit in mangroves' NIR can be attributed to the narrower spectrum of the Landsat NIR which was intended to avoid heavy water contamination (Li et al., 2017). The spectral bandwidth of Landsat-8 and Sentinel-2 NIR is 0.028 and 0.033 μm, respectively. Other variations between the two sensors can be attributed to factors

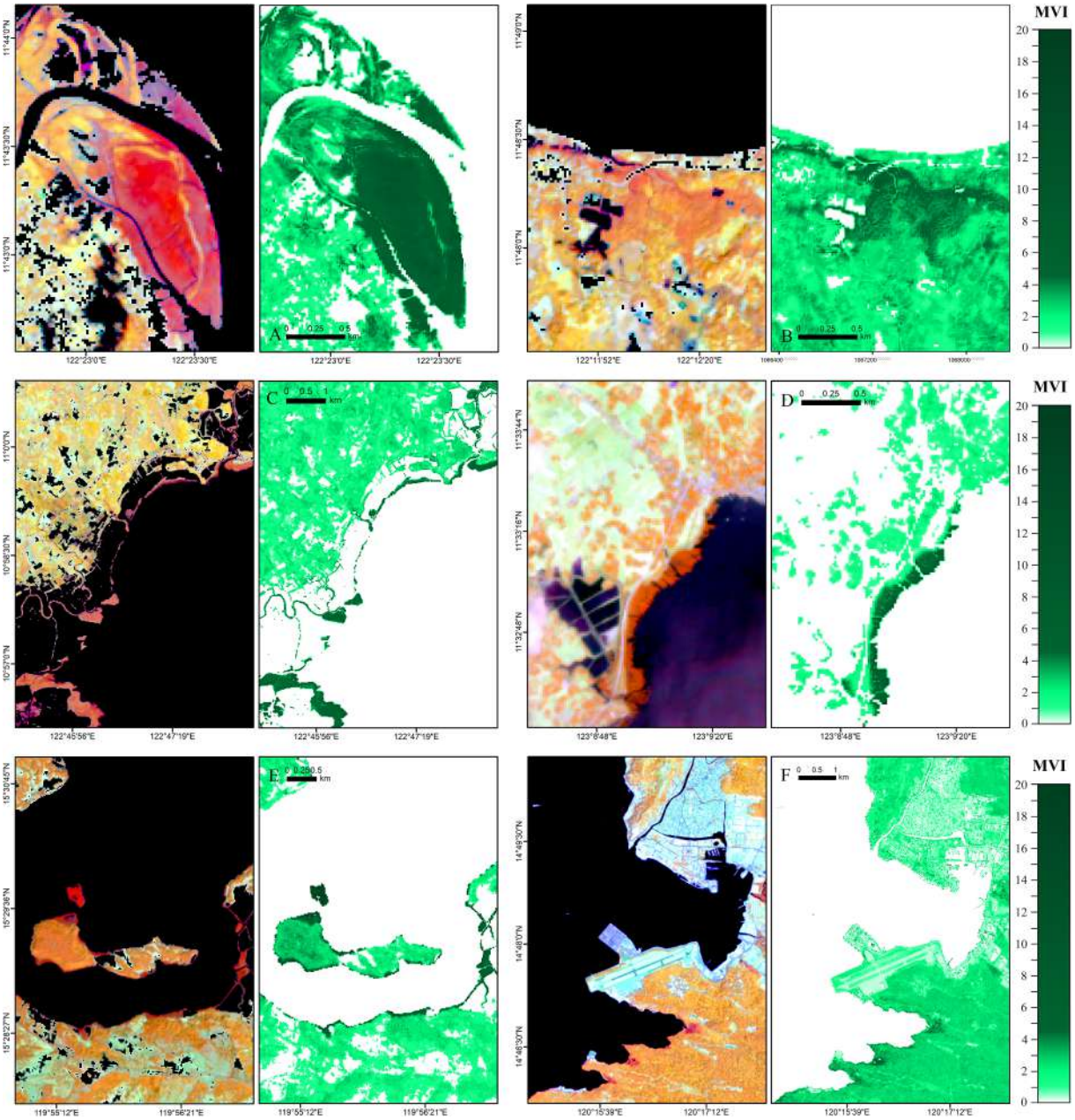

Fig. 7. False color composite (RGB B11-B8-B4) visualization of the atmospherically corrected Sentinel-2 images and the output MVI images in the study sites: (A) Bakhawan Ecopark, Aklan, (B) Katunggan-It Ibajay Ecopark, Aklan, (C) Banate Bay, Iloilo, (D) Bancal Bay, Iloilo, (E) Masinloc in Zambales and (F) Triboa Mangrove Park, Subic in Bataan.

such as heterogeneous terrain, mixed pixels (Runge and Grosse, 2019) and the algorithms used in converting TOA to surface reflectance (Claverie et al., 2018). Between the three classes shown in Fig. 11, the green and SWIR1 values are both lowest in mangroves, as previously observed in Coron-Busuanga dataset. Low green values will help discriminate mangrove greenness while low SWIR1 values separate vegetation from non-vegetation, and moisture-rich vegetation from dry vegetation. The NIR values are more scattered within the mangrove class as the selected sample plots have different cover density.

The MVI formula was applied to Landsat data using the equivalent green, NIR and SWIR1 bands (Fig. 12). The Landsat MVI and Sentinel-2 MVI generated comparable mangrove maps, with similar locations of mangrove forests being highlighted as seen in Fig. 12-B. The Landsat threshold was found to be close with Sentinel-2, with a minimum MVI value of 4.5 and a mean value of 8.6 (Fig. 12-A). Most sample plots, however, have higher Landsat MVI than Sentinel which can be attributed to the observed differences in Fig. 11. Meanwhile, the mean Sentinel-2 MVI from Calauit plots is 7.4 which is very close to the mean MVI obtained from the main Coron-Busuanga Island (7.5). Similar to Sentinel, the 4.5 minimum threshold for Landsat can already discriminate the mangrove areas from bare soil, built-up, terrestrial forest and other terrestrial vegetation cover. However, the obtained maximum MVI threshold of non-mangrove vegetation pixels reach 4.5, so it is suggested to use 4.6 as the safe minimum threshold for Landsat-based MVI mangrove mapping in the selected site.

3.6. Comparison with general vegetation indices

NDVI, LAI and FVC are good indicators of vegetation health. FVC corresponds to the gap fraction for nadir direction, used to separate vegetation and soil in energy balance processes including temperature and evapotranspiration. It is one of the basic ecological characteristics

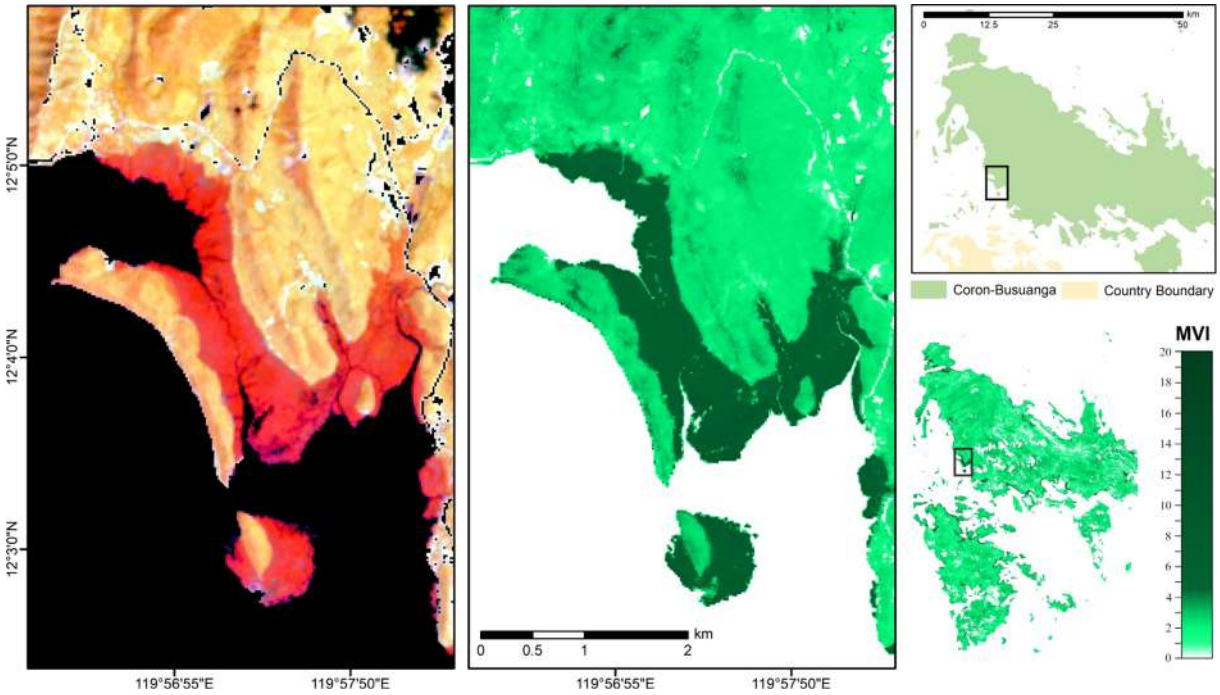

Fig. 8. Comparison of the false color (RGB B11-B8-B4) visualization of the atmospherically corrected Sentinel-2 image (leftmost) and the output MVI image (center) in Busuanga. The mangroves are in dark green color while the non-mangroves are in white to lighter green. The MVI clearly delineated both the nearshore and upstream mangroves by a threshold of 4.5.

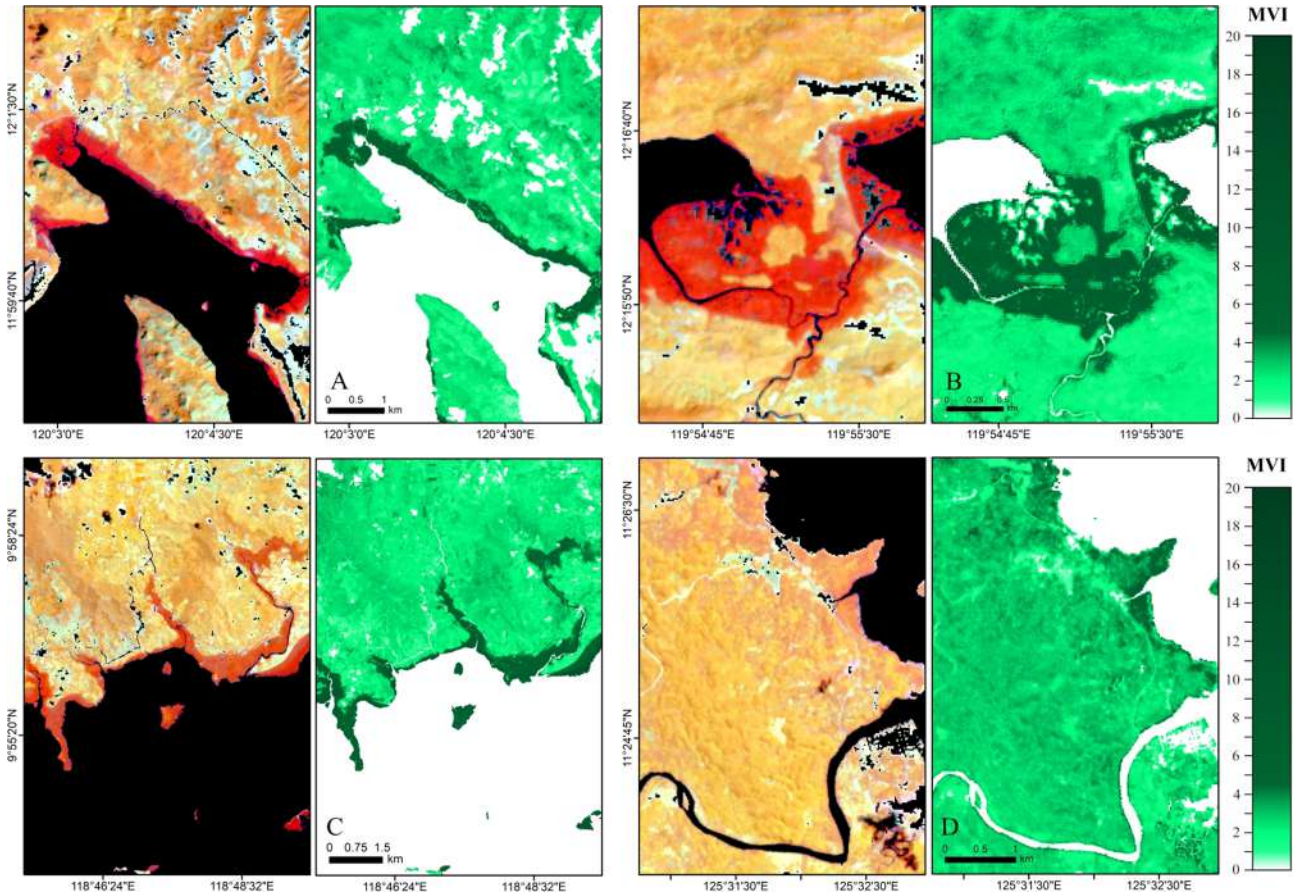

Fig. 9. False color composite (RGB B11-B8-B4) visualization of the atmospherically corrected Sentinel-2 images and the output MVI images in: (A) Bintuan, Coron, (B) Calauit, Busuanga, (C) Bacungan, Puerto Princesa, Palawan and (D) Eastern Samar.

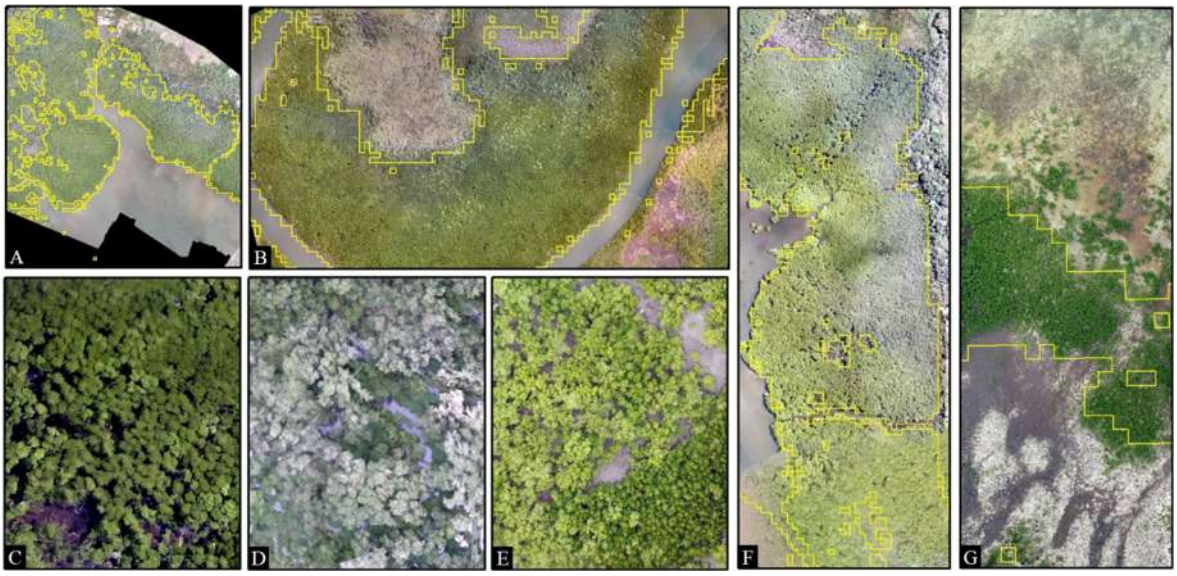

Fig. 10. Drone acquired orthophotos covering the some of the study sites: (A) Coron, (B) Puerto Princesa, (C) Caluit Island, (D) KII Ecopark, (E) Bancal Bay, (F) Busuanga and (G) Eastern Samar. All sites have drone data except Masinloc, Zambales which was validated using mangrove field inventory. The output MVI mangrove shapefile (yellow polygons, A, B, F, and G) were overlaid in the drone images. Phantom 3, Phantom 4 and Sensefly eBee fixed wing drones were used to acquire the RGB image.

Table 4
MVI input bands and the corresponding band wavelengths for Landsat-8 OLI and Sentinel-2.

Multispectral band	Landsat-8		Sentinel-2	
	Band No.	Wavelength (nm)	Band No.	Wavelength (nm)
Green	B3	533–590	B3	543–578
NIR	B5	851–879	B8	785–900
SWIR1	B6	1,567–1,651	B11	1565–1655

Table 5
Accuracy of MVI in discriminating mangroves from non-mangrove pixels, computed using mangrove validation pixels from drone orthophotos and field-acquired tree locations. The highest accuracy was derived from Palawan sites (Coron, Busuanga and Puerto Princesa) while the lowest values were derived from Katunggan-It Ibajay, Aklan and Eastern Samar, two of the smallest study sites.

Study Site	Coverage of Validation Data	Accuracy (%)
Coron-Busuanga	Calauit Island	94
	Bintuan (Coron)	96
	Sagrada and Bogtong (Busuanga)	100
Puerto Princesa, Palawan	Bacungan	98
Panay Island	Banate Bay, Iloilo	90
	Bancal Bay, Iloilo	98
	Katunggan-It Ibajay, Aklan	80
	Bakhawan Ecopark, Aklan	96
Zambales	Triboa Mangrove Park, Subic	87
	Baloganon, Masinloc	90
Eastern Samar	Balangkayan	80
Fukido, Ishigaki	Fukido Mangrove Park	92
	Overall Average Accuracy	92

which can provide quantitative information of the vegetation coverage status on the ground (Li et al, 2015). LAI is defined as half the developed area of photosynthetically active elements of the vegetation per unit horizontal ground area. Variations of LAI in mangrove ecosystems reflects the different environmental forces acting upon each location (Araujo et al, 1997). There are limitations in using of NDVI, LAI and FVC for vegetation discrimination because similar index values can be obtained for all healthy vegetation, regardless of forest type and mangroves species composition (Alsaaideh et al., 2013; Kongwongjan, et al, 2012). The NDVI, LAI and FVC images are shown with MVI in Fig. 13. Unlike other vegetation indices, MVI is a mangrove-specific index which can distinguish mangrove from non-mangrove vegetation. High NDVI means healthier and greener vegetation, and similarly, high MVI can reflect healthier mangrove leaf structures (higher NIR reflectance) and more leaf green pigments (higher green reflectance). Higher MVI can also signify efficient radiation absorption by the water in healthy leaves which can be detected in the SWIR region. Candidate stressed mangrove trees from the study sites gave lower MVI values, while totally damaged and dead trees generated an MVI value outside the mangrove threshold (MVI $<$ 4.5).

The study further analyzed if the MVI range (4.5 and higher) is specifically dependent on mangrove health, so as to conclude if (a) increasing MVI level always means increasing mangrove vigour or (b) increasing MVI means higher probability of a land cover pixel being a mangrove, as affected by canopy greenness and moisture. To facilitate this analysis, candidate mangrove pixels were obtained from two forest types: riverine and fringe mangrove forests. Fringe mangrove forests are directly exposed to the tides and sea waves, while riverine mangroves are flooded by most high tides and dry up at most low tides. Although fringe mangroves are more inundated, the condition within riverine forest are more optimal for healthier growth because of freshwater runoff, nutrient influx, moderate salinity level (Ewel et al, 1998) and low tidal energy (Cunha-Lignon et al, 2011). Riverine mangroves are reported to be among the most productive trees (Ewel et al, 1998) which are significantly denser than the fringe type (Nugroho et al., 2019).

The result shows that mean LAI, FVC, and NDVI are all higher in the riverine forest (Table 6) in agreement with previous studies. The trend for mean MVI is opposite, which is higher in the fringe forests (MVI = 8.9) than in the riverine (MVI = 6.7). This implies that the difference in inundation and background moisture properties between the two forest types could have affected the mangrove MVI values more than leaf health, as reflected by lower mean LAI, FVC and NDVI in the fringe mangroves.

Only riverine mangroves MVI and FVC have moderate positive correlation (r = 0.5), while correlation values between MVI and LAI (r = 0.4) and NDVI (r = 0.04) are lower. The positive correlation of

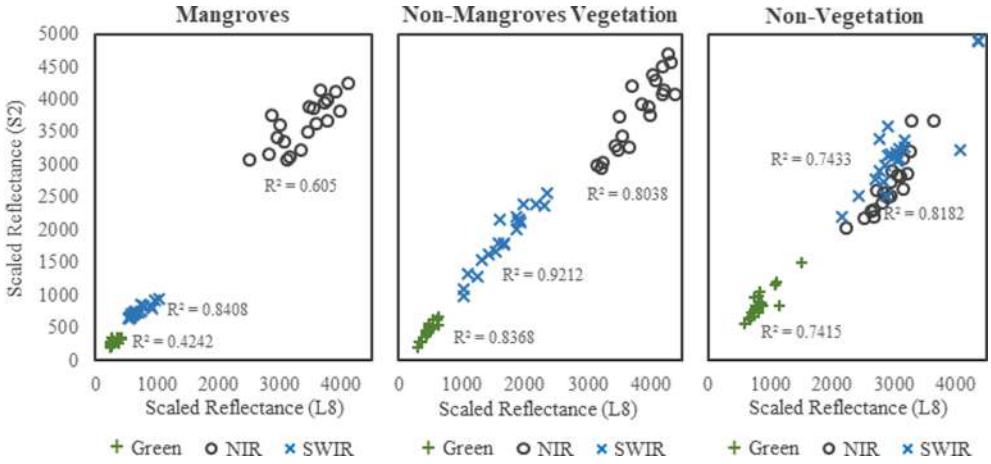

Fig. 11. Spectral fit of the green, NIR and SWIR1 bands between the mangroves and non-mangroves classes derived from atmospherically corrected Landsat-8 and Sentinel-2 images of Calauit Island acquired February 15, 2016 and February 12, 2016.

MVI with FVC and LAI regardless of mangrove forest type implies that all of these indices can reflect the presence and size of a plant photosynthetic area where the leaf greenness and moisture information are obtained. The correlation of NDVI with MVI is higher in the fringe forest (r = 0.3) which could be attributed to the full structural development of seafront mangroves species due to frequent flooding (Cunha-Lignon et al, 2011).

MVI is positively correlated with health indicators such as LAI, FVC and NDVI but was also found to be sensitive to biophysical variations within different mangrove forest types. It was observed that higher MVI values reflects higher probability of an image pixel to be a 'mangrove' rather than solely indicating better vegetation health. Greener vegetation, more leaf water content, and added effect of background soil moisture in the SWIR region as affected by its coastal habitat (Zhang and Tian, 2013) will result to higher MVI. Nevertheless, mangroves captured with less background moisture during low tide will still generate an MVI within the mangrove threshold due to their ability to store enough moisture in the leaves (Camilleri and Ribi, 1983; Nguyen et al, 2017; Reef and Lovelock, 2014). In riverine and other landward mangrove forests, the available less-saline water sources become the main source of water in the xylem as a mechanism to avoid cavitation and regulate water loss (Reef and Lovelock, 2014).

3.7. Comparison with Sentinel-2 derived Chlorophyll-a and canopy water

The chlorophyll-a (C_a) and canopy water (C_w) layers were derived from Sentinel-2 through the SNAP biophysical toolbox SNAP toolbox using tested, generic algorithms based on specific radiative transfer models. C_a is considered as the central photosynthesis pigment as it is a constituent of the photosynthetic reaction center. C_w content is defined as the mass of water per unit ground area, which also relies on the water absorption features centered at 970 nm, 1,200 nm, 1,450 nm and 1,950 nm (Raven et al. 1992). Sentinel's C_w and C_a determine greenness and canopy moisture content which are similar to the biophysical variables considered in generating MVI. For this reason, the study identified the correlation of MVI's greenness equation (NIR-green) with C_a, MVI's moisture equation (SWIR1-green) with C_w, and the output MVI with C_a and C_w. The Sentinel-2 derived C_a and C_w are already quality-controlled data generated using validated models (Jacquemoud and Baret, 1990; Newnham and Burt, 2001; Fourty and Baret, 1997;

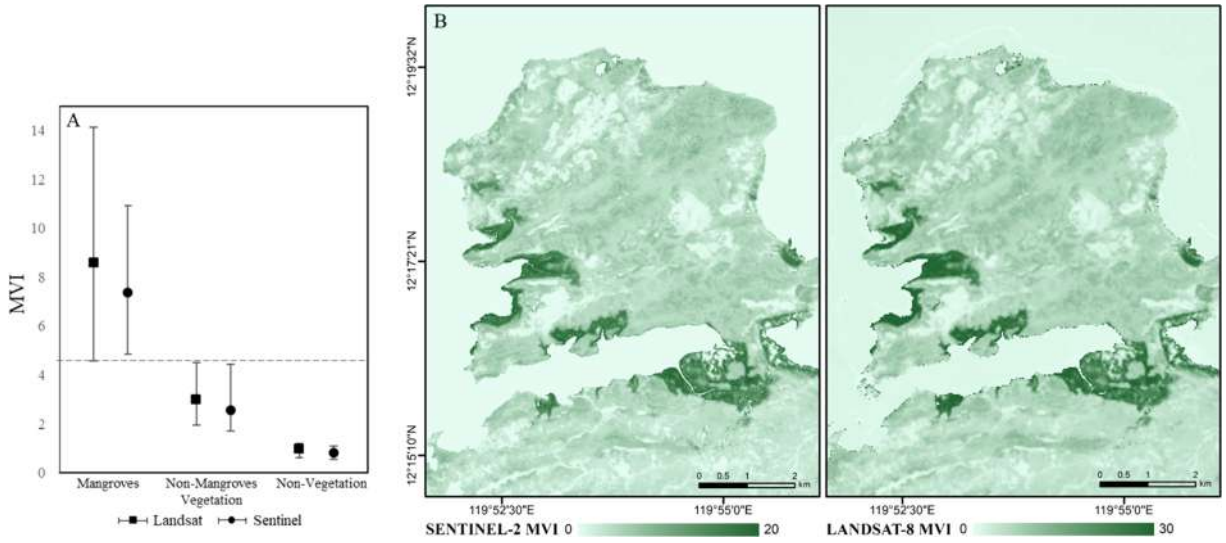

Fig. 12. A. Mean, maximum and minimum Landsat and Sentinel MVI values of mangroves, non-mangroves vegetation and non-vegetation land cover in Calauit Island, Busuanga (graph, left). The minimum threshold for mangrove MVI was observed to be 4.5, but an optimal threshold of 4.6 is suggested as the maximum threshold of non-mangrove vegetation is also 4.5 (Landsat). Overall, the Landsat MVI has wider threshold range than Sentinel-derived MVI. **B.** MVI images generated for Sentinel (map, left) and Landsat (map, right) using the equivalent green, NIR and SWIR bands. The locations of the mangrove areas are found to be similar in both data despite the difference in spatial resolution.

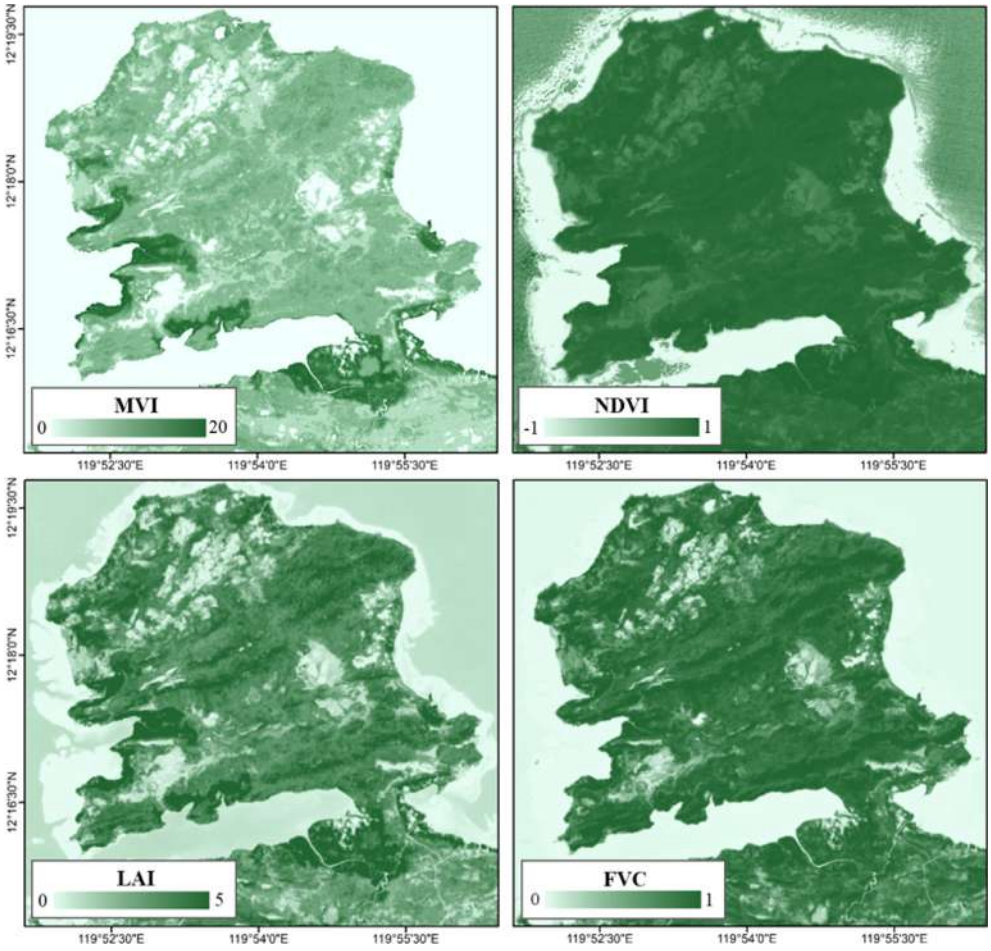

Fig. 13. Mangrove Vegetation Index (MVI) and the generated vegetation indices from Sentinel-2: NDVI, LAI and FVC. High index values were observed within vegetation cover such as mangroves and terrestrial forests, except for MVI which generated high index value solely for mangroves and lower values for non-mangrove vegetation.

Table 6
Mean MVI, LAI, FV and NDVI values obtained from riverine and fringe mangrove forests, and correlation ($\alpha = 0.05$) of the three general vegetation indices with the respective MVI generated for each forest type. Higher MVI was obtained from the fringe mangrove type.

Variable	Riverine Mangrove Forest				Fringe Mangrove Forest			
	MVI	LAI	FVC	NDVI	MVI	LAI	FVC	NDVI
Mean index value	6.7	4.1	0.79	0.73	8.9	3.7	0.7	0.69
Correlation (r) with MVI	–	0.4	0.5	0.04	–	0.2	0.3	0.3

Weiss and Baret, 2016). The result shows high correlation ($\alpha = 0.05$) of MVI with C_w ($r = 0.84$) and C_a ($r = 0.63$) which suggest that the MVI can efficiently measure leaf canopy greenness and moisture (Fig. 14). The MVI greenness and moisture equations alone generated moderate to strong linear relationship with C_a ($r = 0.73$) and C_w ($r = 0.6$). As observed with MVI, C_w levels were reported to be affected also by soil moisture (Weiss and Baret, 2016) and this similarity may have sustained the positive correlation between the two data.

3.8. IDL and Google Earth Engine-based MVI mapping

The IDL platform for offline MVI processing was designed to process offline the available Sentinel-2 input data. The user will need to input the directory of the stacked pre-processed Sentinel-2 bands, the scene qualification data, the lower and upper threshold and the directory for the output folder. The output folder will contain the generated products including the MVI vegetation raster (vegetation masked), the MVI mangrove raster (threshold applied) and the Mangrove shapefile that can already be exported to mapping software for quality check and map layout. The processing time is fast, wherein MVI generation for the whole scene covering Coron-Busuanga only took 3 min. Processing of other subsites ranges from 1 to 18 min, depending on the size of terrestrial cover per Sentinel-2 scene. The IDL-based mapper eliminates the manual processes to facilitate faster product generation.

The Google Earth Engine MVI Mapper (Fig. 15) was designed to have a user-friendly interface. The user can select the desire Sentinel-2 tiles, start and end date of data acquisition, and the target products. There are four products initially listed: the RGB image, the False Color Composite image, the masked vegetation raster and the aster and the mangrove raster. The earliest data that can be selected is March 28, 2017 which is the earliest available date for the Sentinel-2 Multi-Spectral Instrument Level-2A datasets in Google Earth Engine catalogue. Similar with the atmospheric correction algorithm applied in the study sites using SNAP, the said database from GEE is also processed with sen2cor. After running the script, the MVI Mapper will display all available images within the date range. With the aid of RGB and FCC, the user can easily navigate and select the best MVI raster layer with minimum cloud, cloud shadow and haze cover. All four products can be downloaded by clicking on the selected image filename.

Both the IDL and GEE MVI Mapper will be available for public use. Continuous improvement and updates will be made by the researchers.

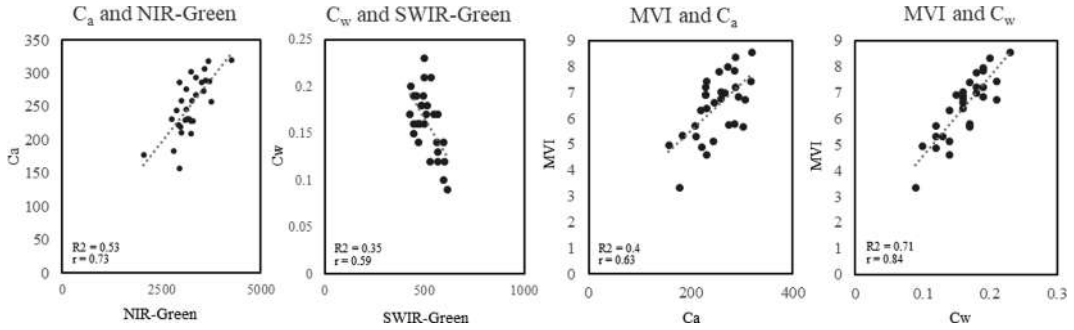

Fig. 14. Correlation between MVI's greenness equation (NIR-green) and Ca, moisture equation (SWIR1-green) and Cw, and resulting MVI values with C_a and C_w. The MVI has moderate positive linear relationship with C_a ($r = 0.63$) and strong positive correlation with C_w ($r = 0.84$). This explains that the MVI is a good indicator of canopy greenness and moisture and can be used an alternative to Sentinel-2 C_a and C_w products for mangrove biophysical analysis. Data for NIR, green and SWIR1 are scaled reflectance (x 10,000).

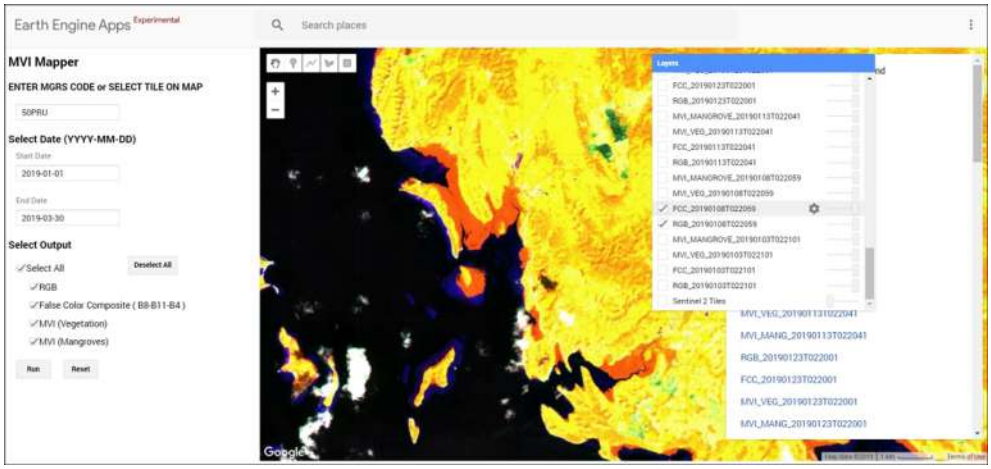

Fig. 15. Google Earth Engine-based Mangrove Mapper interface generated to process online the available Sentinel-2 input data. The four products include RGB, FCC, vegetation MVI raster and mangrove MVI raster. All available data will be displayed.

For the latest version of GEE MVI Mapper, the user can already input the desired lower and upper MVI threshold for mangrove mapping to preview the MVI product before download.

3.9. MVI application for nationwide mapping

Mangroves are distributed throughout the Philippines islands, covered by more than 100 Sentinel tiles. The latest estimate of mangroves in the Philippines is still for year 2016, with a total 220,984 ha (Bunting et al., 2018). The Google Earth Engine GUI was utilized in generating the updated mangrove maps of the country for year 2019. The boundary shapefile for each Military Grid Reference System (MGRS) code for each Sentinel tile was uploaded for faster selection of area. For each tile, the clearest MVI output was selected by displaying it in the GUI map. Based on the results, a combination of clean and contaminated MVIs are obtained within the said year.

Users must navigate first the list of the displayed result (Fig. 15, right panel) and identify the image date with no or less clouds, haze and cloud shadows. The thin haze over dense vegetation tend to generate similar values with MVI, although it is not perpetual among all haze cover. The clouds and cloud shadows can conceal the target mangrove areas and thus can affect the total area in case of mangrove mapping. Out of the 107 tiles covering the country, MVI output was downloaded for 87 tiles. Some mangroves areas are found within the overlap of two Sentinel tiles. Most of the clear images were acquired on the months of April (20 tiles), August and September (15 tiles). No MVI image acquired during the wet season was downloaded such as December, January and February due to the persistence of clouds and haze in the images. In areas with persistent clouds and shadows, additional data from other months were used to fill in the data gaps. In the absence of other clear images, some polygons from GMW were used for the remaining gaps. The output MVI layers were cleaned from noise pixels and was merged into a map showing the updated mangrove extent of the Philippines (Fig. 16). A total of 227,808 ha of mangrove area was obtained (2019), close to the previous estimates by GMW 2016 (220,984 ha), lower than Long and Giri (240, 824 ha) and higher than the UP Phil-LIDAR Landsat-based estimate (208,020 ha).

3.10. Application to other mangrove forests in Southeast Asia

The IDL-based MVI Mapper was utilized to test the application of MVI in mapping the mangroves from four other countries in Southeast Asia in addition to the study site in Ishigaki, Japan. These are Thailand, Vietnam, Indonesia and Cambodia. Mangrove forests in Thailand are located on muddy tidal flats at river mouths and along the coasts specifically on the Gulf of Thailand (Pumijumnong, 2014). The selected site for this study is the mangrove forest in Mueang Trat District in Trat, the easternmost province along the Thailand coast. The chosen Vietnam site is the Can Gio mangrove forest located in Ho Chi Minh City while mangrove forest in Kubu Raya Regency, West Kalimantan was chosen for MVI application in Indonesia. Can Gio is the largest restored mangrove forest in Vietnam (Hung et al., 2018) which was recognised as the first biosphere reserve in Vietnam by UNESCO in the year 2000. The terrain is flat and tide is semi-diurnal. The tile covering the mangroves forests in West Kalimantan include protected coastal and riverine mangroves such as those found in Muara Kubu and Batu Ampar. In

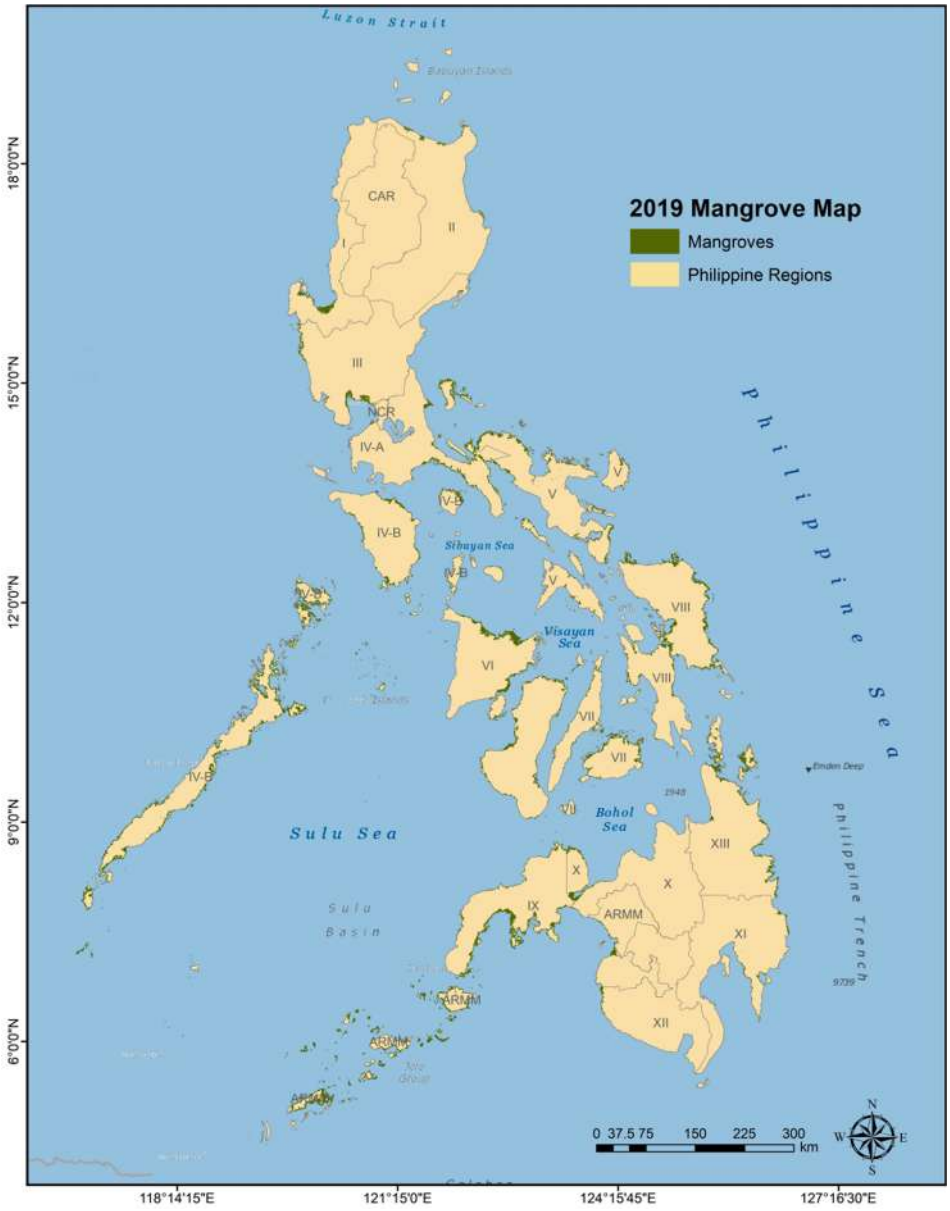

Fig. 16. MVI-based mangrove extent map of the Philippines generated from Sentinel-2 imagery using Google Earth Engine-based MVI Mapper. This map has a spatial resolution of 10 m. The computed total mangrove extent is 227,808 ha for year 2019.

Cambodia, mangroves can only be found in Southwestern part of the country covering four provinces: Koh Kong, Preah Sihanouk, Kompot and Kep (Tieng et al, 2019). Mangrove forest located in Prey Nob was selected which include the Ream National Park.

The selected optimal minimum threshold is 3.5 for the sites in Vietnam and Indonesia, and 3 for Cambodia and Thailand, both situated on the Gulf of Thailand. These thresholds are lower than the 4.5 threshold in the Philippine study sites, but similar and close to average lower threshold (3.5) used for the smaller and less dense mangrove forests in the nationwide mangrove map. Comparison of the Philippine mangrove dataset with the Thailand, Vietnam and Cambodia showed that the differences in the MVI threshold are more driven by the difference in the dividend or the greenness equation than moisture variation. Higher mean NIR reflectance values were recorded from the Philippine site (0.35) as compared to Vietnam (0.31), Thailand (0.28), and Cambodia (0.23). High NIR reflectance is associated to high canopy density, thicker leaves and dense mangrove stands (Patterson, 1986; Zhang et al., 2014). In the Philippines, high mangrove density was previously observed from sample sites with FVC values ranging from 0.7 to 0.79 in fringe and riverine mangrove stands, respectively (Table 6). Meanwhile, the FVC of Vietnam, Thailand, and Cambodia is lower, with mean values of 0.67, 0.62, and 0.56, respectively. Sites with drier mangrove substrates will also result to lower MVI values due to the increase in SWIR1 reflectance, thus increasing the MVI denominator value. This was the factor observed in Indonesia, with mean NIR (0.36) and mean FVC (0.74) values close to that of the Philippines, but with higher moisture equation difference due to higher SWIR1 mean reflectance (0.1) compared to the later (0.07). To facilitate faster selection of threshold, the researchers added a threshold setting option in the GEE MVI Mapper to allow users to preview the MVI output per selected threshold as overlaid to the false color images.

Using IDL-based MVI Mapper, a total of 8,010 ha of mangroves was computed in Trat, Thailand, close to the previously estimated value of 8,190 ha for year 2017 using Landsat data (Pimple et al., 2018), and lower than GMW's estimate of 8,375 for year 2016 (Bunting et al., 2018). For Can Gio, Vietnam, the MVI-based mangrove area estimate is 35,353 ha, close to the estimated values of 35,000 ha in 2017 (HCMC, 2017), and lower than the estimated 38,164 ha in 2016 by GMW

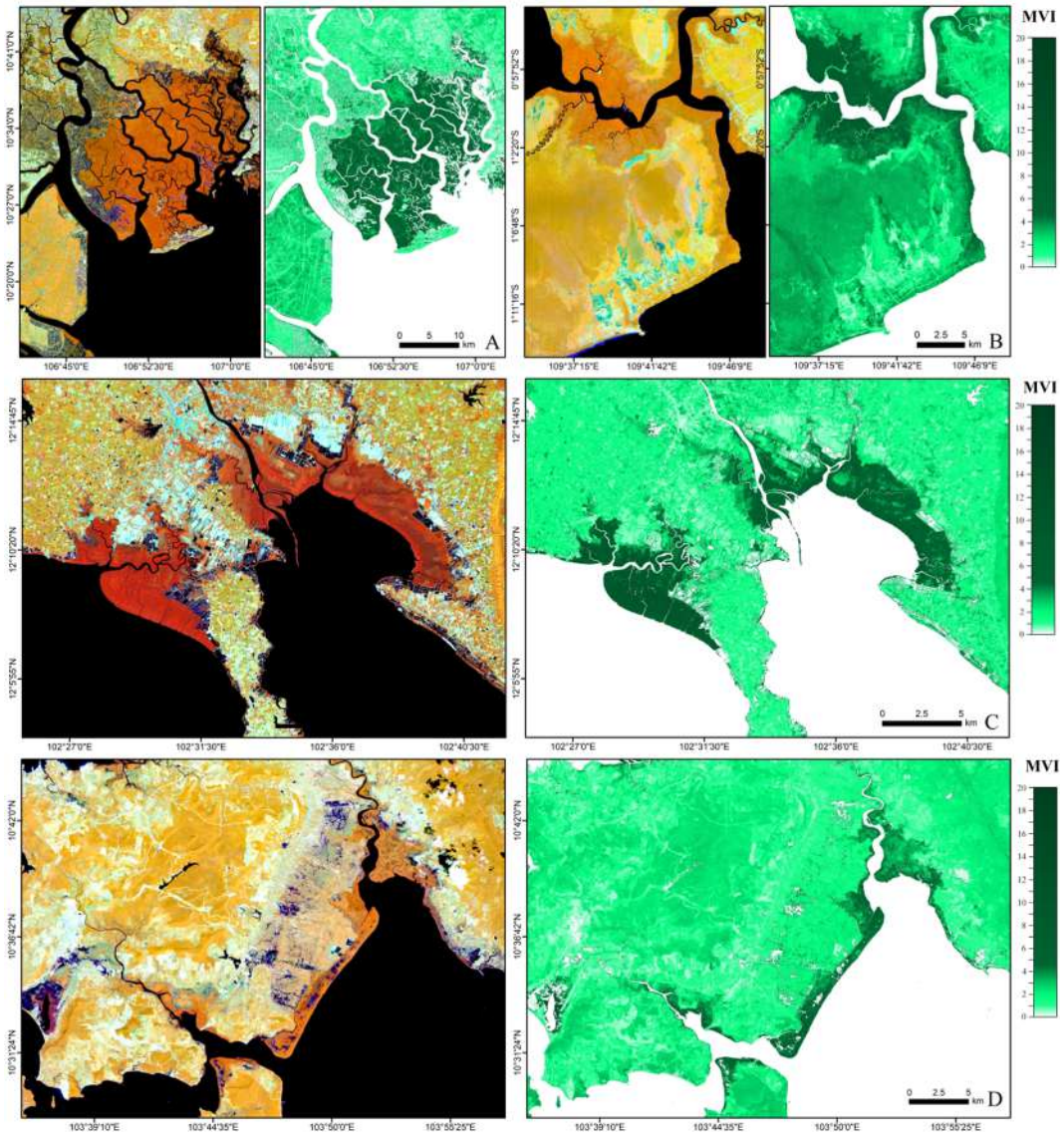

Fig. 17. False color composite visualization and MVI images of generated from Sentinel-2 covering (A) Can Gio Mangrove Forest, Ho Chi Minh City, Vietnam, (B) Muara Kubu and Batu Ampar, West Kalimantan, Indonesia, (C) Mueang Trat District, Trat, Thailand, and (D) Prey Nob, Cambodia. A different threshold was selected for each study site due to the unique coastal environment.

(Bunting et al., 2018) and in 2011 using SPOT 4 and 5 images: 40, 074 ha (Pham et al., 2019). The estimate for the Cambodia site varies based on MVI for year 2019 (6,688 ha), GMW map for year 2016 (9,520 ha) and Landsat-based Random Forest (RF) classified map for years 2014–2015 (13,891) (Tieng et al, 2019). For Indonesia, the total area of the mangrove region shown in Fig. 17 is 17,176 ha. Data cleaning was done due to the persistence of haze and cloud in the images, especially for the Indonesia site.

3.11. Application to mangrove forests outside Asia

The MVI maps of three additional sites namely Baía de São José, Amazon Coast in Brazil, Mabokweni in Tazania, and Prince Regent National Park in Western Australia were generated using the IDL software. Baía de São José is a bay in northeastern Brazil housing the Maranhão mangroves. The area is known to be macrotidal, with tidal amplitude between 4 m and 7.5 m (Souza-Filho, 2005). Meanwhile, mangrove forests in Mabokweni, Tazania occurred along the continental coast of Eastern Africa which houses greater diversity of mangrove species than those located in the west. The third mangrove site is Prince Regent National Park, a UNESCO Biosphere Reserve newly incorporated to the Kimberley National Park. The mangroves in the Kimberly coast occurs in tidal flats, tidal creeks, spits, high-tidal alluvial fans, or in rocky-shore ravines (Cresswell and Semeniuk, 2011).

The mangrove sites of Baía de São José, Mabokweni and Prince Regent National Park (Fig. 18) were found to have an optimum minimum threshold of 3 for MVI mapping. This threshold is similar with that of Prey Nob, Cambodia and Trat, Thailand (Table 7). Compared with the Philippines, the mean MVI generated by said sites are lower, with MVI = 4, 6.5 and 5.7, respectively. The lowest mean MVI (MVI = 4) was computed from Baía de São José, the site with high tidal amplitude. Among the three, the lowest SWIR (0.07) was obtained from Prince Regent National Park which could be induced by the presence of freshwater seepages in the Kimberley Coast (Cresswell and Semeniuk, 2011). The FVC and NIR is also lower compared to that of the Philippines. The FVC of Baía de São José, Mabokweni, and Regent National Park are 0.64, 059, and 0.51, respectively, while Philippine sites' FVC is above 7. The total mangrove areas of the site coverage as shown in Fig. 18 are 21,984 ha for Baía de São José, 824 ha for Mabokweni, and 13,926 ha for Regent National Park.

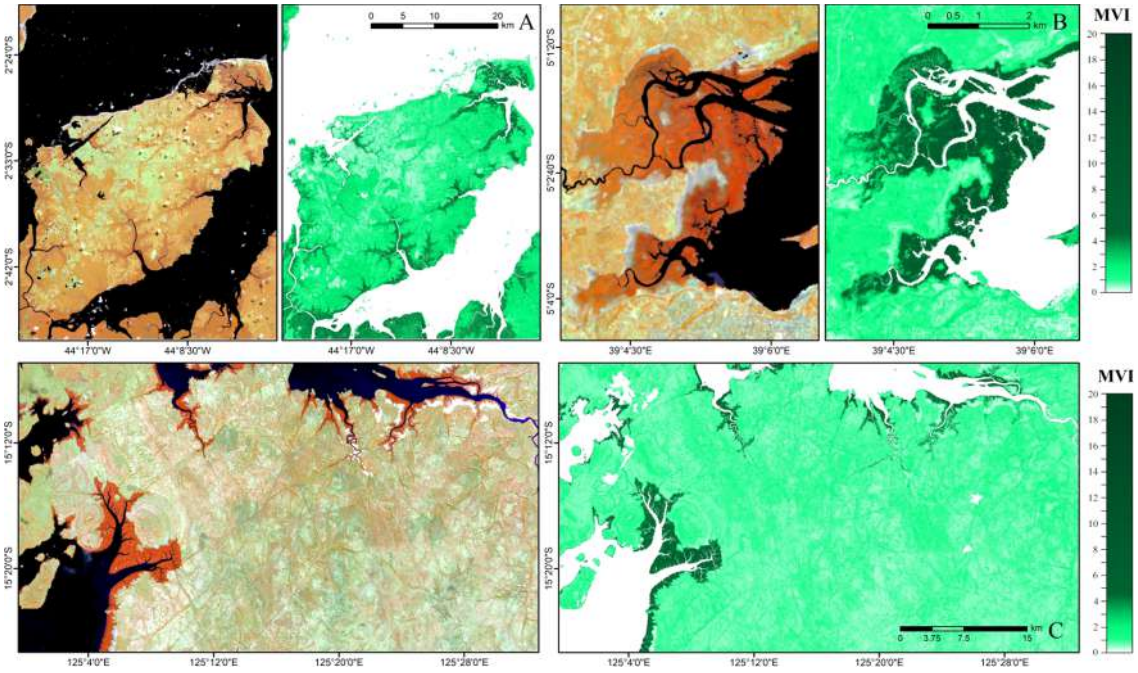

Fig. 18. False color composite visualization and Sentinel-2 MVI images covering three mangrove sites outside Asia: (A) Baía de São José, Amazon Coast, Brazil, (B) Mabokweni, Tazania, and (C) Prince Regent National Park, Western Australia. Similar optimum lower MVI mangrove threshold were computed between the mangrove sites.

There is no clear pattern on the minimum MVI threshold on the basis of latitudinal differences (Table 7). The lower MVI threshold was found to have a very narrow range from 3 to 3.5, despite differences in mangrove typology and geographical coordinates among the sites. This observation highlights the potential of MVI for global-scale mangrove mapping using standard sets of thresholds. Mabokweni and Prince Regent National Park, both estuarine mangroves, utilized a threshold of 3. Mangrove thriving near estuaries and rivers are known to receive higher amount of nutrients but may also be limited by factors such as slow rate of belowground production (Lovelock et al, 2009). Meanwhile, delta mangroves in the Vietnam and Indonesia sites were best mapped using a threshold of 3.5.

3.12. Index uncertainties due to tidal level and rainfall

The occurrence and magnitude of variations in mangrove area and mean MVI values due to differences in tidal and rainfall data were analyzed using multi-temporal data. MVI-derived mangrove area and mean mangrove MVI were examined against biophysical parameters, namely, FVC and C_w, and meteorological data, namely, precipitation (daily), 3-day aggregated precipitation, and tide level. Results show that satellite data acquired during the lowest tide among the dataset for Coron and Busuanga (−0.07 m) and Siargao (0.62 m) have generated the highest FVC and MVI-mapped mangrove areas (Table 8). FVC can provide quantitative information of the vegetation coverage status on the ground (Li et al, 2015). Higher FVC values during the lowest tide indicate detection of more mangrove vegetation canopy which will then affect the computation of MVI. Lower mangrove area estimates were obtained with increased tidal level from −0.07 m to 0.4 m for Coron and Busuanga. However, the magnitude of difference is low, ranging from minus 2.76–6.4 ha. This observation reflects the efficiency of MVI to map mangroves during low to mid-level tides even with the same lower MVI threshold. However, during higher tide events (0.68 m), the area difference reaches to minus 23 ha for Busuanga and minus 43 ha for Coron as more mangroves are submerged and FVC is lower. This variation could be reduced by selecting a lower minimum MVI threshold for Sentinel-2 images acquired during higher tide. In example, using 7 as the minimum threshold for Siargao data collected on a lower tide and adjusting it to 6 for data collected on a higher tide yielded very close results (978 ha and 976 ha), as compared to using the same threshold for both data (Table 8, Siargao). Lowering the threshold allows inclusion of all mangroves within the tidal frame.

The tidal differences have also affected the NIR and SWIR reflectance, and the output MVI values. The data with the lowest tide resulted to the highest mean NIR values for all sites (Table 8). With increasing tide level, reduction in the NIR values was observed which is

Table 7
The selected mangrove forest sites in Southeast Asia, South America, Africa and Australia, and their respective geographical locations, dominant mangrove typology, and the lower minimum threshold utilized to map the mangroves.

Region	Mangrove Site	Latitude	Longitude	Mangrove Type	MVI Threshold
Southeast Asia	Philippines (countrywide mean threshold)	12°52′47″ N	121°46′26.5″ E	Fringe	3.5
	Can Gio Mangrove Forest, Vietnam	10°33′39.3″ N	106°52′08.6″ E	Delta	3.5
	West Kalimantan, Indonesia	0°39′59.0″ S	109°31′00.6″ E	Delta	3.5
	Prey Nob, Cambodia	10°40′43.9″ N	103°52′54.1″ E	Fringe	3
	Mueang Trat District, Trat, Thailand	12°08′59.1″ N	102°29′39.7″ E	Fringe/Estuary	3
South America	Baia do Arraial, Amazon Coast, Brazil	2°39′32.3″ S	44°09′49.2″ W	Delta	3
Africa	Mabokweni, Tazania	5°02′13.3″ S	39°04′27.1″ E	Estuary	3
Australia	Prince Regent National Park, Western Australia	15°16′49.9″S	125°08′04.8″E	Estuary	3

Table 8
Mean MVI metrics and the respective precipitation, tide, FVC, and C_w data for each satellite image acquired during the dry and wet seasons in Busuanga, Coron, and Siargao. Consistently, the highest mangrove area and highest mean mangrove MVI occurred for satellite data with the highest FVC value. These data will high FVC were all acquired during days with lower tide level. As tide level increases, the mangrove area and mean mangrove MVI decreases as more mangrove and mangrove parts are submerged in water. The effect of varying precipitation level during and before the data acquisition date yielded insignificant change in the canopy water content through C_w, and thus had minimal effect on mangrove reflectance and MVI values.

Busuanga	Meteorological Data				Biophysical Data		MVI Metrics				
	Season	Total Daily Precipitation (mm)	Total 3-day Precipitation (mm)	Tide level (m)	Mean FVC	Mean C_w	Min. MVI Threshold	Mangrove Area (ha)	Mean NIR	Mean SWIR	Mean Mangrove MVI
Jan 08, 2019	Dry	0	0.19	0.4	0.75	0.16	4.3	277.07	3421	751	8.1
Jun 12, 2019	Wet	1.9	33.1	0.68	0.74	0.15	4.3	256.74	3192	819	7.4
Dec 29, 2019	Wet (Late)	0	15.2	−0.07	0.76	0.16	4.3	279.83	3489	763	8.6
Jan 23, 2020	Dry	0	0	0.22	0.74	0.16	4.3	273.41	3332	735	8.2
Coron	Meteorological Data				Biophysical Data		MVI Metrics				
	Season	Total Daily Precipitation (mm)	Total 3-day Precipitation (mm)	Tide level (m)	Mean FVC	Mean C_w	Min. MVI Threshold	Mangrove Area (ha)	Mean NIR	Mean SWIR	Mean Mangrove MVI
Jan 08, 2019	Dry	0	0.15	0.4	0.70	0.14	4.3	253.8	3061	713	7.6
Jun 12, 2019	Wet	5.9	36.8	0.68	0.67	0.12	4.3	215.56	2766	788	6.5
Dec 29, 2019	Wet (Late)	0	23.31	−0.07	0.73	0.14	4.3	258.76	3305	779	7.8
Jan 23, 2020	Dry	0	0	0.22	0.71	0.14	4.3	254.92	3168	736	7.7
Siargao	Meteorological Data				Biophysical Data		MVI Metrics				
	Season	Total Daily Precipitation (mm)	Total 3-day Precipitation (mm)	Tide level (m)	Mean FVC	Mean C_w	Min. MVI Threshold	Mangrove Area (ha)	Mean NIR	Mean SWIR	Mean Mangrove MVI
Feb 21, 2019	Dry	0	3.35	0.62	0.74	0.15	7	978	3286	743	12.8
Aug 10, 2019	Wet	0	0.06	0.98	0.73	0.15	7	867	3127	739	10.1
							6	976	3117	752	9.7

mainly due to the submersion of some mangroves and mangrove parts (Jia et al., 2019). As discussed earlier, reduction in NIR can lower the MVI formula dividend or the greenness information value, resulting to lower MVI. This can be observed in all sites where lower mean NIR yielded to lower mean mangrove MVI. The lowest mean NIR and mean MVI values were consistently recorded during high tide. The maximum difference between mangrove MVI values recorded during low to mid-level tides is only 0.5 for Busuanga and 0.2 for Coron. The Sentinel-2 images taken on January 2019 and January 2020, both acquired during lower tide levels, generated close MVI values of 8.1 and 8.2, respectively despite the one-year gap. The differences between per-site MVI values are higher during higher tides, with up to minus 1.2 for Busuanga, 1.3 for Coron, and 2.7 for Siargao.

High SWIR values were recorded during the highest tide and lowest tide, and lower during the mid-level tides. The difference among the SWIR1 values per site is lower than of NIR values, indicating that it has less effect on the MVI variation. SWIR1 value is known to be affected by soil background moisture (Herrmann et al., 2010) which is dependent on the soil properties. Mangrove substrate is known to be frequently waterlogged and is usually consist of clay loam with high water retention capacity. High SWIR reflectance of mangroves during the lowest tide could be connected with leaf water deficit (Kokaly et al., 2009), although some mangroves can store enough leaf moisture (Camilleri and Ribi, 1983; Nguyen et al, 2017).

Meanwhile, the effect of rainfall to the canopy water content is very minimal, with a difference of 0 to 1 in the C_w values despite varying amount of daily and 3-day aggregated precipitation. The data acquired December 29, 2019 and January 23, 2020 in Coron and Busuanga produced comparable MVI values and mangrove areas although up to 23 mm of rain occurred prior to acquisition of the earlier satellite images. The Coron-Busuanga and Siargao sites exhibit different tidal patterns during some months of the year due to their opposing locations, but the reducing effect of higher tides to the mean MVI values were similarly observed. This was taken in consideration in selecting the dates of satellite images used in the nationwide mapping.

4. Conclusion

This study provides an index built using green, NIR, and SWIR1 reflectance bands for discriminating mangrove from non-mangroves cover. Mangrove Vegetation Index, or MVI, measures the probability of a pixel to be a 'mangrove' by extracting the greenness and moisture information from the Sentinel-2 green, NIR and SWIR1 bands. The optimal MVI threshold from the study sites is from 4.5 to 20, but the lower threshold may be adjusted depending on the canopy density and coastal environment of the site. MVI have successfully discriminated visually and statistically the mangroves from non-mangroves cover types such as bare soil, built-up, terrestrial forest and terrestrial non-forest vegetation. The average index accuracy was 92%, validated through high resolution drone photos and field inventory data. Low to mid-level tidal height induced minimal variation on MVI values, while satellite data acquired during higher tides have less mean MVI due to reduced fractional cover of mangrove vegetation, affecting both the MVI greenness and moisture equations. Lowering the MVI threshold is necessary unless only satellite data collected during lower tidal events will be selected.

Stressed mangrove trees gave lower MVI values, while totally damaged and dead trees generated an MVI value outside the mangrove threshold. However, comparison with vegetation health indicators such as NDVI, FVC and LAI in riverine and fringe mangrove forests suggested that the MVI value does not always increase with increasing vegetation health, but rather increase with higher probability of a pixel being classified as 'mangroves' based on the greenness and moisture information. This was further validated by correlating the MVI values with Sentinel-2 SNAP-derived chlorophyll-a (C_a) and canopy water content (C_w). MVI was strongly and positively correlated with C_w and C_a which suggest that the MVI can efficiently measure greenness and moisture in the canopy level. The MVI formula was applied to Landsat-8 data using the equivalent green, NIR and SWIR1 data. The Landsat and Sentinel-2 bands had moderate agreement in the green and NIR regions, and high in the SWIR1 region. The Landsat MVI had wider threshold range and has higher values than Sentinel-2 in most of the sample plots,

but the optimal minimum threshold is the same which is 4.5 and/or 4.6 for the case of the Philippines. Similar mangrove area locations were detected between the two sensors.

This study developed two mangrove mapping automation tools, the IDL-based and Google Earth Engine-based MVI Mapper. The IDL MVI Mapper can be used offline when the input data is already downloaded, while the Google Earth Engine GUI can be operated online without the need to locally download the input Sentinel-2 bands. Further, the study mapped the mangrove extent in the Philippines using the GEE workflow to generate an updated mangrove map with higher resolution (10 m). The MVI was also applied to four other countries in Southeast Asia: Thailand, Vietnam, Indonesia and Cambodia. Although lower minimum thresholds were selected compared with Philippine sites, the MVI can still separate the mangrove from non-mangrove cover with the said adjusted thresholds, generating mangrove area estimates close to previous estimates obtained from previous studies in the said sites. Further application of MVI to mangrove forests in Brazil, Tazania, and Western Australia showed similar thresholds with the mangrove sites in Southeast Asia. Other MVI applications such as mangrove spatio-temporal analysis, change detection and automatic site-specific threshold detection can be further explored in future works. MVI can be used for rapid and accurate mangrove mapping because of the non-complex input data, simple index calculation, high initial index accuracy, universality of the index which is applicable to other satellite data, and the availability of automation tools.

Author contributions

Alvin Baloloy and Ariel Blanco conceptualized the ideas and design of the study including data collection and analysis; Raymund Sta. Ana contributed in the automation of the mapping workflow; and Kazuo Nadaoka assisted in assessing and reviewing the applicability of the index. All authors contributed in writing the manuscript.

Declaration of competing interest

The authors declare that they have no known competing financial interests or personal relationships that could have appeared to influence the work reported in this paper.

Acknowledgements

This research work was done under the 'The Project for Comprehensive Assessment and Conservation of Blue Carbon Ecosystems and their Services in the Coral Triangle (BlueCARES) funded by Japan International Cooperation Agency (JICA) and Japan Science and Technology Agency (JST) under the SATREPS Program. Most of the validation data were acquired during the 'Integrated Assessment and Modelling of Blue Carbon Ecosystems for Conservation and Adaptive Management' (IAMBlueCECAM) Project 1: Mangrove Remote Sensing using LiDAR, RADAR, Multispectral and Hyperspectral Data (MaRS, Project No. 04038) funded by the DOST Philippine Council for Industry, Energy and Emerging Technology Research and Development (PCIEERD). Utmost acknowledgement is given to the Nationwide Detailed Resource Assessment Using LiDAR (Phil-LiDAR 2) for the Masinloc field inventory data. Further, the researchers would like to thank the Environmental Systems Applications of Geomatics Engineering (EnviSAGE) laboratory for the equipment and assistance given in conducting the study.

Appendix A. Supplementary material

Supplementary data to this article can be found online at https://doi.org/10.1016/j.isprsjprs.2020.06.001.

References

Alongi, D.M., 2002. Present state and future of the world's mangrove forests. Environ. Conserv. 29, 331–349. https://doi.org/10.1017/S0376892902000231.

Al-Saidi, A., Fukuzawa, Y., Ueno, M., Baba, S., Kawamitsu, Y., 2009. Temporal and vertical variations in photosynthetic drivers in mangrove canopies, Okinawa. Japan. Plant Prod. Sci. 12, 336–340. https://doi.org/10.1626/pps.12.336.

Alsaaideh, B., Al-Hanbali, A., Tateishi, R., Kobayashi, T., Thanh Hoan, N., 2013. Mangrove Forests Mapping in the Southern Part of Japan Using Landsat ETM + with DEM. J. Geogr. Inf. Syst. 5, 369–377. https://doi.org/10.4236/jgis.2013.54035.

Araujo, R.J., Jaramillo, J.C., Snedaker, S.C., 1997. LAI and leaf size differences in two red mangrove forest types in South Florida. Bulletin of Marine Science 60 (3), 643–647.

Ashraf, M.A., Maah, M.J., Yusoff, I. 2011. Introduction to Remote Sensing of biomass, biomass and Remote Sensing of biomass. Dr. Islam Atazadeh (Ed.), ISBN: 978-953-307-490-0. InTech. https://doi.org/10.5772/16462.

Basheer, M.A., Kafrawy, S.B., Mekawy, A., 2019. Identification of mangrove plant using hyperspectral remote sensing data along the Red Sea. Egypt. Egyptian J. Aquatic Biol. Fisheries. 23, 27–36. https://doi.org/10.21608/ejabf.2019.25932.

Bowman, K.P., 2004. An introduction to computer programming using Interactive Data Language (IDL). Department of Atmospheric Sciences Texas A&M University.

Bunting, P., Rosenqvist, A., Lucas, R., Rebelo, L.-M., Hilarides, L., Thomas, N., Hardy, A., Itoh, T., Shimada, M., Finlayson, C.M., 2018. The Global Mangrove Watch – a new 2010 global baseline of mangrove extent. Remote Sens. 10, 1669. https://doi.org/10.3390/rs10101669.

Cahoon, D.R., Hensel, P., Rybczyk, J., Mckee, K.L., Proffitt, C.E., Perez, B.C., 2003. Mass tree mortality leads to mangrove peat collapse at Bay Islands, Honduras after Hurricane Mitch. J. Ecol. 91, 1093–1105. https://doi.org/10.1046/j.1365-2745.2003.00841.x.

Camilleri, J.C., Ribi, G., 1983. Leaf thickness of mangroves (*Rhizophora mangle*) growing in different salinities. Biotropica. 15, 139–141. https://doi.org/10.2307/2387959.

Cierniewski, J., Kuśnierek, K., 2010. Influence of several soil properties on soil surface reflectance. Quaestiones Geographicae. 29, 13–25. https://doi.org/10.2478/v10117-010-0002-9.

Claverie, M., Ju, J., Masek, J.G., Dungan, J.L., Vermote, E.F., Roger, J.C., Skakun, S.V., Justice, C., 2018. The harmonized Landsat and Sentinel-2 surface reflectance dataset. Remote Sens. Environ. 219, 145–161. https://doi.org/10.1016/j.rse.2018.09.002.

Clough, B.F., 1993. Conservation and sustainable utilization of mangrove forests and their present state of conservation in the South-east Asia/Pacific Region. Mangrove Ecosystems Technical Reports No. 1. International Society for Mangrove Ecosystems, Okinawa, Japan, pp. 202.

Cresswell, I.D., Semeniuk, V., 2011. Mangroves of the Kimberley Coast: ecological patterns in a tropical ria coast setting. J R Soc. West Aust. 94, 213–237. http://hdl.handle.net/102.100.100/104152?index=1.

Crooks, S., Herr, D., Tamelander, J., Laffoley, D., Vandever, J., 2011. Mitigating climate change through restoration and management of coastal wetlands and near-shore marine ecosystems: challenges and opportunities. Environment Department, Paper 121. World Bank, Washington, DC.

Cunha-Lignon, M., Coelho Jr., C., Almeida, R., Menghini, R.P., Schaeffer-Novelli, Y., Cintrón, G., Dahdouh-Guebas, F., 2011. Characterisation of mangrove forest types in view of conservation and management: a review of mangals at the Cananéia region, São Paulo State. Brazil. J. Coast. Res. 64, 349–353.

Dangan-Galon, F., Dolorosa, R.G., Sespeñe, J.S., Mendoza, N., 2016. Diversity and structural complexity of mangrove forest along Puerto Princesa Bay, Palawan Island, Philippines. J. Marine Island Cultures 5, 118–125. https://doi.org/10.1016/j.imic.2016.09.001.

Diop, E.S, Conservation and sustainable utilization of mangrove forests and their present state of conservation in Latin America and Africa regions. Technical Reports, Volume 3. Okinawa, Japan. International Society for Mangrove Ecosystems, 1993, 262.

Ellison, J.C. 2000. How South Pacific mangroves may respond to predicted climate change and sea level rise. Chapter 15, pages 289-301, In: Gillespie, A., and Burns, W. (eds), Climate change in the South Pacific: impacts and responses in Australia, New Zealand, and small islands states. Kluwer Academic Publishers, Dordrecht, Netherlands. https://doi.org/10.1007/0-306-47981-8_16.

European Space Agency. The Copernicus Open Access Hub. Available online: (accessed on August 2018).

Deilmai, B.R., Ahmad, B.B., Zabihi, H., 2014. Comparison of two classification methods (MLC and SVM) to extract land use and land cover in Johor Malaysia. IOP Conf. Ser. Earth Environ. Sci. 20, 1–6. https://doi.org/10.1088/1755-1315/20/1/012052.

Ewel, K.C., Twilley, R.R., Ong, J.E., 1998. Different kinds of mangrove forests provide different goods and services. Global Ecol. Biogeogr. 7, 83–89. https://doi.org/10.1111/j.1466-8238.1998.00275.x.

Food Agric. Organ. U. N. (FAO). 2003. Status and trends in mangrove area extent worldwide. Work. Pap. FRA 63, FAO, Rome,Italy. 14.

Farnsworth, E.J., Ellison, A.M., 1998. The global conservation status of mangroves. Oceanogr. Lit. Rev. 1, 138–139. http://reforestation.elti.org/resource/212/.

Field, C.D., 1995. Impact of expected climate change on mangroves. Hydrobiologia. 295, 75. https://doi.org/10.1007/BF00029113.

Fourty, T., Baret, F. 1997. Amélioration de la précision des coefficients d'absorption spécifiquede la matière sèche et des pigments photosynthétiques. INRA Bioclimatologie. 35.

Garces, L.R., Pido, M.D., Tupper, M.H., Silvestre, G.T., 2012. Evaluating the management effectiveness of three marine protected areas in the Calamianes Island, Palawan Province, Philippines: Process, selected results and their implications for planning and management. Ocean. Coast. Manage. 1–9. https://doi.org/10.1016/j.ocecoaman.2012.07.014.

Ghandi, S., Jones, T.G., 2019. Identifying mangrove deforestation hotspots in South Asia Southeast Asia and Asia-Pacific. Remote Sens. 11, 728. https://doi.org/10.3390/rs11060728.
Giri, C., Muhlhausen, J., 2008. Mangrove forest distribution and dynamics in Madagascar (1975–2005). Sensors 8, 2104–2117. https://doi.org/10.3390/s8042104.
Giri, C., Ochieng, E., Tieszen, L.L, Zhu, Z., Singh, A., Loveland, T., Masek, J., Duke, N., 2011. Status and distribution of mangrove forests of the world using earth observation satellite data. Glob. Ecol. Biogeogr. 20, 154–159. https://doi.org/10.1111/j.1466-8238.2010.00584.x.
Górska, A., Lazor, J.W., Zwieniecka, A.K., Benway, C., Zwieniecki, M.A., 2010. The capacity for nitrate regulation of root hydraulic properties correlates with species' nitrate uptake rates. Plant Soil. 337, 447–455. https://doi.org/10.1007/s11104-010-0540-x.
Green, R.O., Pavri, B.E., Chrien, T.G., 2003. On-Orbit radiometric and spectral calibration characteristics of EO-1 Hyperion derived with an underflight of AVIRIS and in situ measurements at Salar de Arizaro. Argentina. IEEE T Geosci Remote. 41, 1194–1203. https://doi.org/10.1109/TGRS.2003.813204.
Gupta, K., Mukhopadhyah, A., Giri, S., Chanda, A., Majumdar, S.D., Samanta, S., Mitra, D., Samal, R.N., Pattnaik, A.K., Hazra, S., 2018. An Index for discrimination of mangroves from non-mangroves using Landsat 8 OLI imagery. MethodsX. 5, 1129–1139. https://doi.org/10.1016/j.mex.2018.09.011.
HCMC, 2017. Decision No. 3901 on approving the areas of forest and land in HCM city in 2016. Ho Chi Minh: The people's committee of HCM city.
Herrmann, I., Karnieli, A., Bonfil, D.J., Cohen, Y., Alchanatis, V., 2010. V. SWIR-based spectral indices for assessing nitrogen content in potato fields. Int. J. Remote Sens. 31, 5127–5143. https://doi.org/10.1080/01431160903283892.
Hoa, N.H., Binh, T.D., 2016. Using Landsat imagery and vegetation indices differencing to detect mangroves change: a case study in Thai Thuy District, Thai Province. J. of For. Sci. Tech. 5, 59–66.
Hopper, M. 2007. WXTide32 software. http://WXTide32.com.
Huete, A.R. 2004. Remote Sensing for Environmental Monitoring in: Environmental Monitoring and Characterization. https://doi.org/10.1016/B978-012064477-3/50013-8.
Huete, A.R., 1988. A soil adjusted vegetation index (SAVI). Remote Sens. Environ. 25, 295–309. https://doi.org/10.1016/0034-4257(88)90106-X.
Hung, T.T., Huyen, D.T., Tu, T.A., Desmet, M., 2018. Presence of trace elements in sediment of Can Gio mangrove forest, Ho Chi Minh City Vietnam. Vietnam J. Earth Sci. 41, 25–31. https://doi.org/10.15625/0866-7187/41/1/13543.
Jacquemoud, S., Baret, F., 1990. Prospect - a model of leaf optical-properties spectra. Remote Sens. Environ. 34, 75–91. https://doi.org/10.1016/0034-4257(90)90100-Z.
Jia, M., Wang, Z., Wang, C., Mao, D., Zhang, Y., 2019. A new vegetation index to detect periodically submerged Mangrove forest using Single-Tide Sentinel-2 Imagery. Remote Sens. 11, 2043. https://doi.org/10.3390/rs11172043.
Jusoff, K., 2006. Individual mangrove species identification and mapping in Port Klang using airborne hyperspectral imaging. J. Sustain. Sci. Manage. 1, 27–36.
Kamal, M., Phinn, S., 2011. Hyperspectral data for mangrove species mapping: a comparison of pixel-based and object based approach. Remote Sens. 3, 2222–2242. https://doi.org/10.3390/rs3102222.
Kamaruzaman, J., Kasawani, I., 2007. Imaging Spectrometry on Mangrove Species Identification and Mapping in Malaysia. WSEAS Trans. Biol. Biomed. 4, 118–126. http://psasir.upm.edu.my/id/eprint/7723.
Kanniah, K.D., Sheikhi, A., Cracknell, A.P., Goh, H.C., Tan, K.P., Ho, C.S., Rasli, F.N., 2015. Satellite images for monitoring mangrove cover changes in a fast growing economic region in Southern Peninsular Malaysia. Remote Sens. 7, 14360–14385. https://doi.org/10.3390/rs71114360.
Kathiresan, K., Bingham, B.L., 2001. Biology of mangroves and mangrove ecosystems. Adv. Marine Biol. 40, 81–251. https://doi.org/10.1016/S0065-2881(01)40003-4.
Kokaly, R.F., Asner, G.P., Ollinger, S.V., Martin, M.E., Wessman, C.A., 2009. Characterizing canopy biochemistry from imaging spectroscopy and its application to ecosystem studies. Remote Sens. Environ. 113, 78–91. https://doi.org/10.1016/j.rse.2008.10.018.
Kongwongjan, J., Suwanprasit, C., Thongchumnum, P. 2012. Comparison of vegetation indices for mangrove mapping using THEOS data. Proceedings of the Asia-Pacific Advanced Network. 33, 56-64. http://dx.doi.org/10.7125/APAN.33.6.
Kovacs, J.M., Wang, J., Blanco-Correa, M., 2001. Mapping disturbances in a mangrove forest using multi-date Landsat TM imagery. Environ. Manag. 27, 763–776. https://doi.org/10.1007/s002670010186.
Kumar, T., Mandal, A., Dutta, D., Nagaraja, R., Dadhwal, V.K., 2019. Geocarto Int. 34, 415–442. https://doi.org/10.1080/10106049.2017.1408699.
Lawas, L.M. 1974. Economic study on alternative uses of mangrove swamps: bakawan production or fish ponds. In: Proceedings of Indo-Pacific Fishery Council, 65-69. 15th Session. 18-27 October 1972, Wellington, New Zealand, Section 2 Bangkok, FAO.
Li, S., Ganguly, S., Dungan, J.L., Wang, W., 2017. Nemani, R.R. Sentinel-2 MSI radiometric characterization and cross-calibration with Landsat-8 OLI. Adv. Remote Sens. 6, 147. https://doi.org/10.4236/ars.2017.62011.
Li, Y., Wang, H., Li, X.B., 2015. Fractional vegetation cover estimation based on an improved selective endmember spectral mixture model. PLoS ONE 10, 4. https://doi.org/10.1371/journal.pone.0124608.
Lin, P., Fu, Qin, 1995. Environment, ecology and economic utilization of mangrove in China. Higher Education Press, Beijing, China.
Liu, K., Li, X., Shi, X., Wang, S., 2008. Monitoring mangrove changes using remote sensing and GIS data with decision-tree learning. Wetlands 28, 336–346. https://doi.org/10.1672/06-91.1.
Long, J.B., Giri, C., 2011. Mapping the Philippines' mangrove forests using Landsat imagery. Sensors 11, 2972–2981. https://doi.org/10.3390/s110302972.
Lovelock, C.E., Ball, M.C., Martin, K.C., Ferrer, I.C., 2009. Nutrient enrichment increases mortality of mangroves. PLoS ONE 4, e5600. https://doi.org/10.1371/journal.pone.0005600.
Lu, D., Weng, Q.A., 2007. A survey of image classification methods and techniques for improving classification performance. Int. J. Remote Sens. 28, 823–870. https://doi.org/10.1080/01431160600746456.
Ma, L., Li, M., Ma, X., Cheng, L., Du, P., Liu, Y., 2017. A review of supervised object-based land-cover image classification. ISPRS J. Photogramm. Remote Sens. 130, 277–293. https://doi.org/10.1016/j.isprsjprs.2017.06.001.
Main-Knorn, M., Pflug, B., Debaecker, V., Louis, J. 2015. Calibration and validation plan for the L2A processor and products of the Sentinel-2 Mission. ISPRS Ann. Photogramm. Remote Sens. Spat. Inf. Sci. 40, 1249-1255. http://doi.org/10.5194/isprsarchives-XL-7-W3-1249-2015.
Manna, S., Raychaudhuri, B., 2018. Mapping distribution of Sundarban mangroves using Sentinel-2 data and new spectral metric for detecting their health condition. Geocarto Int. 1–20. https://doi.org/10.1080/10106049.2018.1520923.
Newnham, G.J., Burt, T., 2001. Validation of leaf reflectance and transmittance model for three agricultural crop species. IEEE Trans. Geosci. Remote Sens. 2976–2978. https://doi.org/10.1109/IGARSS.2001.978227.
Nguyen, H.T., Meir, P., Sack, L., Evans, J.R., Oliveira, R.S., Ball, M., 2017. Leaf water storage increases with salinity and aridity in the mangrove Avicennia marina: integration of leaf structure, osmotic adjustment and access to multiple water sources. Plant Cell Environ. 40, 1576–1579. https://doi.org/10.1111/pce.12962.
Nugroho, T.S., Fahrudin, A., Yulianda, F., Bengen, D., 2019. Structure and composition of riverine and fringe mangroves at Muara Kubu protected areas. AACL Bioflux 12, 378–393. http://www.bioflux.com.ro/docs/2019.378-393.pdf.
Patterson, W.G., 1986. Mangrove Community Boundary Interpretation and Detection of Areal Changes in Marco Island, Florida: Application of Digital Image Processing and Remote Sensing Techniques, U.S. Fish Wildlife Service Biolog. Rep. 86, 1–87.
PCAFNRRD, 1991. The Philippines recommends for mangrove production and harvesting. In: Forestry Research Series. Philippine Council for Agriculture, Forestry and Natural Resources Research and Development, Department of Science and Technology, Los Banos, Laguna, pp. 96 74.
Pekel, J.F., Cottam, A., Gorelick, N., Belward, A.S., 2016. High-resolution mapping of global surface water and its long-term changes. Nature 540, 418–422. https://doi.org/10.1038/nature20584.
Pham, L.T.H., Vo, T.Q., Dang, T.D., Nguyen, U.T.N., 2019. Monitoring mangrove association changes in the Can Gio biosphere reserve and implications for management. Remote Sens. Appl. Soc. Environ. 13, 298–305. https://doi.org/10.1016/j.rsase.2018.11.009.
Pimple, U., Simonetti, D., Sitthi, A., Pungkul, S., Leadprathom, K., Skupek, H., Som-ard, J., Gond, V., Towprayoon, S., 2018. Google earth engine based three decadal landsat imagery analysis for mapping of mangrove forests and its surroundings in the Trat province of Thailand. J. Comput. Commun. 6, 247–264. https://doi.org/10.4236/jcc.2018.61025.
Prasad, K.A., Gnanappazham, 2015. Multiple statistical approaches for the discrimination of mangrove species of Rhizophoraceae using transformed field and laboratory hyperspectral data. Geocarto Int. 31, 891–912. https://doi.org/10.1080/10106049.2015.1094521.
Primavera, J.H., 2000. Development and conservation of Philippine mangroves: Institutional issues. Ecol. Econ. 35, 91–106. https://doi.org/10.1016/S0921-8009(00)00170-1.
Primavera, J.H., 2005. Mangroves, Fishponds, and the Quest for Sustainability. Science 310, 57–59. https://doi.org/10.1126/science.1115179.
Pumijumnong, N. 2014. Mangrove Forests in Thailand. In: Faridah-Hanum I., Latiff A., Hakeem K., Ozturk M. (eds) Mangrove Ecosystems of Asia. Springer, New York, NY. https://doi.org/10.1007/978-1-4614-8582-7_4.
Raven, P.H., Evert, R.F., Eichhorn, S.E., 1992. Biology of plants. W. H. Freemann & Company Press, New York, NY.
Razali, S.M., Nuruddin, A.A., Lion, M., 2019. Mangrove vegetation health assessment based on remote sensing indices for Tanjung Piai, Malay Peninsular. J. Landsc. Ecol. 12, 26–40. https://doi.org/10.2478/jlecol-2019-0008.
Reef, R., Lovelock, C.E., 2014. Regulation of water balance in mangroves. Ann Bot. 115, 385–395. https://doi.org/10.1093/aob/mcu174.
Romañach, S.S., DeAngelis, D.L., Koh, H.L., Li, Y., Teh, S.Y., Raja Barizan, R.S., Zhai, L., 2018. Conservation and restoration of mangroves: Global status, perspectives, and prognosis. Ocean Coast. Manag. 154, 72–82. https://doi.org/10.1016/j.ocecoaman.2018.01.009.
Roslani, M.A., Mustapha, M.A., Lihan, T., Wan Juliana, W.A., 2003. Classification of mangroves vegetation species using texture analysis on RapidEye satellite imagery. AIP Conference Proc. 1571, 480. https://doi.org/10.1063/1.4858701.
Rouse, J.W., Has, R.H., Schell, J.A., Deering, D.W. 1973. Monitoring vegetation systems in the Great Plains with ERTS. In Proceedings of the Third ERTS Symposium (NASA), Washington, DC, USA, SP-351 I, 309-317.
Rullan-Silva, C.D., Olthoff, A.E., Delgado de la Mata, J.A., Pajares-Alonso, J.A., 2013. Remote Monitoring of Forest Insect Defoliation - A Review. For. Syst. 22, 377. https://doi.org/10.5424/fs/2013223-04417.
Runge, A., Grosse, G., 2019. Comparing spectral characteristics of Landsat-8 and Sentinel-2 same-day data for arctic-boreal regions. Remote Sens. 11, 1–29. https://doi.org/10.3390/rs11141730.
Sandalo, R.M., Baltazar, T. 1997. The Palawan Biosphere Reserve: Philippines. Working Papers No. 19, 1997. Paris, France: UNESCO. South-South Cooperation Programme for Environmentally Sound Socio-Economic Development in the Humid Tropics.
Schmidt, G., Jenkerson, C., Masek, J., Vermote, E., Gao, F., 2013. Landsat ecosystem disturbance adaptive processing system (LEDAPS) algorithm description. US Geolog. Survey. https://doi.org/10.3133/ofr20131057.
Sharma, S., Yasuoka, J., Nakamura, T., Watanabe, A., Nadaoka, K. 2014. The Role of

hydroperiod, soil moisture and distance from the river mouth on soil organic matter in Fukido Mangrove Forest, Ishigaki Island, Japan. In Proceeding of the Intl. Conf. on Advances In Applied Science and Environmental Engineering. 2014. ISBN: 978-1-63248-004-0.

Sikdar, D., Banerjee, A., Das, P., Datta, S., 2016. Biodegradation of Acenaphthene Using Two Different Isolated Bacteria: Comparative Analysis and Optimization Using Artificial Neural Network. Environ. Pollut. Protect. 1, 12–22. https://doi.org/10.22606/epp.2016.11002.

Souza-Filho, P.W., 2005. Costa de manguezais de macromaré da Amazônia: cenários morfológicos, mapeamento e quantificação de áreas usando dados de sensores remotos. Revista Brasileira de Geofísica. 23, 427–435. https://doi.org/10.1590/S0102-261X2005000400006.

Spalding, M., Blasco, F., Field C.,eds. 1997. World Mangrove Atlas. Okinawa, JP. Int. Soc. Mangrove Ecosyst. 178.

Spalding, M., Kainuma, M., Collins, L. 2010. World Atlas of Mangroves. Earthscan, London, Washington DC, 319.

Tieng, T., Sharma, S., MacKenzie, R.A., Venkattappa, M., Sasaki, N.K., Collin, A. 2019. Mapping mangrove forest cover using Landsat-8 imagery, Sentinel-2, very high resolution images and Google Earth Engine algorithm for entire Cambodia. IOP Conf. Series: Earth and Environmental Science. 266. http://doi.org/doi:10.1088/1755-1315/266/1/012010.

Tomlinson, P.B. 1994. The botany of mangroves. Cambridge, UK: Cambridge University Press. https://doi.org/10.1017/CBO9781139946575.

Tucker, C.J., 1980. Remote sensing of leaf water content in the near infrared. Remote Sens Environ. 10, 13–32.

Tyerman, S. D., Wignes, J. A., Kaiser, B. N. 2017. “Root Hydraulic and Aquaporin Responses to N Availability,” in Plant Aquaporins, eds F. Chaumont and S. Tyerman (Cham: Springer). 207–236.

Veettil, B.K., Pereira, S.R.F., Quang, N.X., 2018. Rapidly diminishing mangrove forests in Myanmar (Burma): A Review. Hydrobiologia. 822, 19–35. https://doi.org/10.1007/s10750-018-3673-1.

Villamayor, B.M.R., Rollon, R.N., Samson, M.S., Albano, G.M.G., Primavera, J.H., 2016. Impact of Haiyan on Philippine mangroves: Implications to the fate of the widespread monospecific Rhizophora plantations against strong typhoons. Ocean Coast Manage. 132, 1–14. https://doi.org/10.1016/j.ocecoaman.2016.07.011.

Wang, D., Wan, B., Qiu, P., Zuo, Z., Wang, R., Wu, X., 2018. Evaluating the Performance of Sentinel-2, Landsat 8 and Pléiades-1 in Mapping Mangrove Extent and Species. Remote Sens. 10, 1468. https://doi.org/10.3390/rs10091468.

Weiss M., Baret F. 2016. S2ToolBox Level 2 products: LAI, FAPAR, FCOVER. Accessed on 12 September 2018. Available online: http://step.esa.int/docs/extra/ATBD_S2ToolBox_L2B_V1.1.pdf.

Winarso, G., Purwanto, A.D., Yuwono, D.M. 2014. New mangrove index as degradation / health indicator using Remote Sensing data: Segara Anakan and Alas Purwo case study. 12th Biennial Conference of Pan Ocean Remote Sensing Conference.

Zhang, C., Kovacs, J.M., Liu, Y., Flores-Verdugo, F., Flores-de-Santiag, F., 2014. Separating Mangrove Species and Conditions Using Laboratory Hyperspectral Data: A Case Study of a Degraded Mangrove Forest of the Mexican Pacific. Remote Sens. 6, 11673–11688. https://doi.org/10.3390/rs61211673.

Zhang, X., Tian, Q., 2013. A mangrove recognition index for remote sensing of mangrove forest from space. Current Sci. 105, 1149–1154.

Zhang, X., Treitz, P.M., Chen, D., Quan, C., Shi, L., Li, X., 2017. Mapping mangrove forests using multi-tidal remotely-sensed data and a decision-tree-based procedure. Int. J. Appl. Earth Obs. Geoinfo. 62, 201–214. https://doi.org/10.1016/j.jag.2017.06.010.